Tao, S., Eglinton, T. I., Zhang, L., Yi, Z., Montluçon, D. B., McIntyre, C. , Yu, M. and Zhao, M. (2018) Temporal variability in composition and fluxes of Yellow River particulate organic matter. *Limnology and Oceanography*, 63(S1), S119-S141. (doi:10.1002/lno.10727)

Temporal variability in composition and fluxes of Yellow River particulate organic matter

Shuqin Tao,[1,2,3] Timothy I. Eglinton,[3,*] Liang Zhang,[4] Zhiwei Yi,[2] Daniel B. Montluçon,[3] Cameron McIntyre,[3,5†] Meng Yu,[1,3] Meixun Zhao[1,*]

[1] Key Laboratory of Marine Chemistry Theory and Technology (Ocean University of China), Ministry of Education/Laboratory for Marine Ecology and Environmental Science, Qingdao National Laboratory for Marine Science and Technology, Qingdao 266071, China

[2] Third Institute of Oceanography, SOA, Xiamen 361005, China

[3] Geological Institute, Department of Earth Sciences, ETH Zürich, 8092 Zürich, Switzerland

[4] State Oceanographic Administration, Xiamen marine environmental monitoring center station, Xiamen 361008, China

[5] Laboratory for Ion Beam Physics, Department of Physics, ETH Zürich, 8093 Zürich, Switzerland

[†] Present address: Scottish Universities Environmental Research Centre (SUERC), G750QF, Glasgow, UK

[*] Corresponding authors:

Timothy I. Eglinton, E-mail: timothy.eglinton@erdw.ethz.ch, Tel.: +41 44 6339291, Fax: +41 44 6331296

Meixun Zhao, E-mail: maxzhao@ouc.edu.cn, Tel.: +86 532 66782103, Fax: +86 532 66782103

Abstract

This study examines temporal variations of the abundance and carbon isotopic characteristics of particulate organic carbon (POC) and specific-source compounds in the context of hydrological variability in the Yellow River. The content and bulk carbon isotopic characteristics (^{13}C and ^{14}C) of POC were relatively uniform over the hydrologic (seasonal) cycle. We attribute these temporally invariant geochemical characteristics to the dominant contribution of loess material to the suspended particulate matter (SPM). In contrast, molecular-level signals revealed that hydrologic conditions exert a significant influence on the proportional contributions of petrogenic and especially fresh plant-derived OC, while pre-aged soil OC is mobilized via deeper erosion processes (e.g., gully erosion, mudslides) and is independent of hydrodynamics and surface runoff. A coupled biomarker-isotope mixing model was applied to estimate the time-varying supply of contemporary/modern biomass, pre-aged soil, and fossil OC components to Chinese marginal seas from the Yellow River. We found that natural (e.g., precipitation) and human-induced (e.g., water and sediment regulation) variations in hydrological regime strongly influence the flux with the magnitude of the corresponding annual fluxes of POC ranging between 0.343±0.122 to 0.581±0.213 Mt/yr, but less strongly infleunce proportions of the different OC constituents. Inter-annual differences in pre-aged soil and fossil OC fluxes imply that extreme climate events (e.g., floods) modulate the exhumation and export of old carbon to the ocean, but the OC homogeneity in the pre-aged mineral soil-dominated watersheds facilitates robust predictions in terms of OC transport dynamics in the past (sediment cores) and in the future.

Keyword: The Yellow River, compound-specific carbon isotopes (^{14}C and ^{13}C),

contemporary OC, pre-aged soil OC, fossil OC, temporal variability

The residence time of biospheric OC in terrestrial reservoirs such as soils can play an important role in buffering variations in atmospheric carbon dioxide concentrations. Erosion, transport and burial of terrestrial OC in continental margin sediments can also result in a long-term carbon sink. Rivers connect terrestrial and marine reservoirs, exporting ~ 0.45 Pg C yr^{-1} (Pg = 1 × 10^{15} g) of organic carbon and ~ 0.26 Pg C yr^{-1} of inorganic carbon to the ocean from various terrestrial sources including plants, soils and weathered rocks (Cole et al. 2007). This corresponds to ~25% of the terrestrial sink for anthropogenic CO_2 emissions (2.8 Pg C/yr; Battin et al., 2009), and thus represents a significant component of both regional and global carbon cycles. Although spatially localized, over prolonged time the net OC fluxes in aquatic systems tend to be greater per unit area than in much of the surrounding land (Cole et al. 2007 and references therein).

POC in river networks is supplied via diverse processes that operate on a range of timescales. In addition of autochthonous production within fluvial systems, relatively fresh (young) terrestrial POC may be mobilized from the land via surface run-off, while of aged OC in deeper mineral soils is remobilized largely through collapse of riverbanks or and erosion of surrounding soils, contributing POC depleted in ^{14}C content to the river (Raymond and Bauer 2001; Blair and Aller 2012; Feng et al. 2013b; Vonk et al. 2014). Riverine POC can be thus considered as a combination of freshly-produced and pre-aged biospheric organic matter augmented by ancient petrogenic OC eroding from bedrock within the drainage basin. The majority of recently-synthesized biospheric OC, such as

plant detritus is rapidly recycled to the atmosphere as CO_2 during fluvial transport (Mayorga et al. 2005; Ward et al. 2013). In contrast, mineral-bound soil and petrogenic OC may be more efficiently exported and buried in coastal environments (Aller et al. 2008; Tao et al. 2016). The balance between remineralization and sequestration of these different components is of importance in determining whether fluvial transport serves as a long-term carbon sink or a source of atmospheric CO_2 (Berner 1982; Aller and Blair 2004; Bianchi 2011). Thus, improved understanding of the composition of riverine OC, as well as the magnitude and timescales of fluvial export, are necessary to develop robust constraints on the terrestrial OC cycle and its links to OC burial in marine environments.

Molecular tools, particularly when coupled with isotopic information, can be used to trace sources and processes acting upon OC in the environment. Although source-specific biomarker compounds are generally trace constituents of POC, their isotopic signatures reflect and are representative of the corresponding carbon source. In particular, the ^{14}C content of biomass will reflect its biological source independent of its metabolism (e.g, autotroph vs. heterotroph), and irrespective of the specific class of biochemical (e.g., lipid, polysaccharide, protein, lignin). Thus, by measuring the ^{14}C content of a source-specific lipid biomarker (e.g., higher plant wax fatty acid) we can gain insights into the isotopic characteristics of the overall OC derived from this source, and hence can assess its contribution to a bulk OC signal. The situation is similar for stable carbon isotopes, although biosynthetic fractionation effects that impart different isotope compositions to different cellular components must also be considered (Schouten et al. 1998; Wiesenberg et al. 2004). Source apportionment approaches involving coupled ^{13}C and ^{14}C measurements on both bulk OC and specific biomarkers have been applied in prior studies (Drenzek et al. 2007;

Drenzek et al. 2009; Feng et al. 2013a; Tao et al. 2015; Tao et al. 2016), and while subject to improvement and refinement, these approaches offer a means to resolve multiple contributions to riverine POC.

Besides, POC sources and transport processes within fluvial systems likely vary both spatially and temporally, being influenced by changes in both the provenance of exported materials and hydrological conditions (e.g., Voss et al., 2015). Moreover, superimposed on natural variability, are changing dynamics in OC export brought about by on-going anthropogenic climate change and perturbations to watersheds and river networks. The latter may result in return of now-dormant OC, held in deep soils or bedrock, to the active carbon cycle. Determining of the nature and magnitude of OC, as well as putative remineralization to CO_2 during or subsequent to transport to the ocean represents an important question for assessment of carbon-climate couplings (Tarnocai et al. 2009; Galy and Eglinton 2011). Molecular-level biomarker [isotope] approaches are particularly powerful as they distinguish 'pre-aged' and 'fossil' sourced OC signatures and enable OC derived from these pools to be traced into fluvial and marine systems where they become admixed with organic matter from other sources (Drenzek et al. 2007; Galy and Eglinton 2011; Gustafsson et al. 2011; Feng et al. 2013a). At present, however, while there is growing information on the ^{13}C and ^{14}C isotopic compositions of terrestrial biomarker compounds exported from different river systems, there is a paucity of information regarding how vary on seasonal or inter-annual timescales (Drenzek et al. 2009; Martin et al. 2013). Thus, long-term measurements ($\geq$ 1 year) are important for understanding how terrestrial-ocean carbon transfer by rivers will be impacted by climate and anthropogenic change.

In this study, we applied a coupled biomarker-isotope approach to investigate time-varying fluxes and sources of OC transported by the Yellow River (Huanghe). A previous study focused on establishing a three end-member mixing model in order to apportion Yellow River suspended POC into three components based on bulk OC and molecular carbon isotopic characteristics (Tao et al. 2015). This study, based on dual carbon isotopic mass balance, concluded that pre-aged (ave. 1770 years ^{14}C age) soil OC (53±12%) and fossil (ave. 24590 years ^{14}C age) OC (31±2%) dominated the annual POC load. The large flux of pre-aged and fossil OC carries important implications for our understanding of OC cycling associated with erosion and carbon export from this globally significant fluvial system to the adjacent marginal sea. Temporal variability in the limited dataset acquired, as this prior study was only examined in the context of uncertainty in end-member compositions, and did not permit in-depth assessment of the degree and nature of temporal variability inherent within the river system. The Yellow River exhibits pronounced inter- and intra-annual variations in sediment and water flux in response to both natural (e.g., East Asian monsoon) and anthropogenic factors (e,g,, dam construction and river flow regulation) (Milliman et al. 1987; Wang et al. 2006; Peng et al. 2010), the impacts of the latter being particularly pronounced over the past 100 years. Comprehensive investigation of anthropogenic influences is thus a prerequisite for understanding current and predicting future OC dynamics of the Yellow River. Building on our prior investigation (Tao et al. 2015), this paper focuses on temporal variations of abundance and carbon isotopic characteristics of bulk OC and specific biomarker compounds in the context of hydrological variability in the river. Using an extended time-series sample set collected

quasi bi-monthly (June 2011 - July 2013) from the main channel near the outlet of the river, we assess how the proportions and fluxes of different OC source components changes on a seasonal and inter-annual basis.

Study areas and methods

Study area

The Yellow River, originating on the Qinghai-Tibet Plateau at an elevation of 4500 m, is the world's fifth longest river, running 5464 km from its source to the Bohai Sea and encompassing a drainage area of 75.2×10^4 km^2 (Fig. 1). The Yellow River basin spans the entire semi-arid and arid region of northern China (Xu et al. 2006), and encompasses diverse geological, geomorphic and ecological gradients from the Tibet Plateau in the upper drainage basin, through the Mu Us desert and the Loess Plateau in the middle basin, to the extensive floodplain of the lower basin (Zhang et al. 1995; Hu et al. 2012a). Precipitation is influenced by the East Asian monsoon and exhibits strong seasonal variability (An 2000). Frequent heavy storms during the wet season (June–September) can account for 50% of annual total precipitation (Wang et al. 2006), forming a distinct summer-autumn natural high flow (NHF) period, whereas intensive ice-melting during the dry season (February–April) can also cause higher runoff in the spring NHF period (Zhang et al. 2013). The monsoon season typically accounts for about 60% and 80% of the annual Yellow River water runoff and TSS export, respectively (Fig. 2; archived data from the Yellow River Water Network; http://www.sdhh.gov.cn/hhsq/).

Experimental methods

All samples were collected from the main channel at Kenli, near the Lijing Hydrological Station (ca. 50 km upstream of the river mouth). Near-surface SPM was collected due to the shallowness of the main channel during most months (0.4–2.0 m; ave. ~1.5m, Wang et al., 2012). Water (typically 120−200 L) was filtered through pre-combusted, pre-weighed 150 mm diameter GF/F filters (nominal pore size of 0.7 μm, Whatman) to recover enough SPM for the bulk and compound-specific carbon isotope analysis.

For bulk POC content, bulk ^{13}C and ^{14}C measurements, small aliquots of freeze-dried, homogenized and acidified SPM were prepared to remove inorganic carbon (Komada et al. 2008). For source-specific biomarker measurement, a detailed description of methods for extraction, purification and isolation of target biomarkers (lipids and lignin derived phenols) was provided by Tao et al. (2015). Briefly, about 50–100 g of freeze-dried and homogenized suspended sediment was solvent-extracted, and after saponification (0.5 M KOH in CH_3OH) the total lipid extract was chromatographically separated to obtain three classes of target *n*-alkyl lipid biomarkers including *n*-fatty acid methyl esters (analyzed as *n*-FAMEs), *n*-alkanes and *n*-alkanols (analyzed as *n*-alkanol acetates). To check purity and for quantification, a small aliquot of each fraction was analyzed by gas chromatography (GC) and another aliquot (<5%) was kept for stable carbon isotopic analysis. The remaining fractions (*n*-alkanes, *n*-alkanol acetates and *n*-FAMEs) were further purified and isolated by preparative capillary gas chromatography (PCGC) prior to compound-specific ^{14}C analysis (Eglinton et al., 1996) using modified protocols described by Tao et al. (2015). Lignin-derived phenols were released from the solvent-extracted SPM residues by microwave-assisted alkaline CuO oxidation (MARS 5; CEM Corporation) (Goñi and

Montgomery 2000). The resulting phenolic monomers were isolated using an HPLC-based method developed for compound-specific ^{14}C analysis (Feng et al. 2013a).

Stable carbon isotopic compositions of bulk OC and source specific biomarkers obtained from each sample were determined in duplicate by a EA-isotope ratio Mass Spectrometry and GC-isotope ratio Mass Spectrometry, respectively, at ETH-Zürich. Results are reported as $\delta^{13}C$ values ($\delta^{13}C_{TOC}$, $\delta^{13}C_{Compound}$) relative to VPDB standard (‰). Their corresponding radiocarbon isotopic compositions were measured on a gas-ion source MICADAS accelerator mass spectrometry (AMS) system at the Laboratory for Ion Beam Physics, ETH Zürich (Ruff et al. 2010; Wacker et al. 2010). All radiocarbon data were expressed as $\Delta^{14}C$ ($\Delta^{14}C_{TOC}$, $\Delta^{14}C_{Compound}$) and corresponding radiocarbon age (years before 1950 AD). All carbon isotopic compositions of *n*-FAMEs and *n*-alkanol acetates were corrected for the contribution of the added methyl (–1000±1‰) and acetyl carbon (–999±1‰), respectively, based on isotopic mass balance in order to derive carbon isotope values and associated errors for underivatized compounds. Analytical uncertainty for ^{14}C analysis of specific compounds isolated with the PCGC was within 40‰ (ave., 12‰) after the error propagation calculation (Hou et al. 2010).

Monte Carlo calculations

This study quantifies temporal variations in relative fractional proportions of three different components (i.e. recently synthesized biomass (f_B), pre-aged mineral soil/loess (f_S) and ^{14}C-free fossil (f_F) OC) in Yellow River suspended POC by applying a three end-member mixing model with two carbon isotopic signals for each end-member ($\delta^{13}C$

and $\Delta^{14}C$).

$$\Delta^{14}C_{POC} = \left[f_B \times \Delta^{14}C_B\right] + \left[f_S \times \Delta^{14}C_S\right] + \left[f_F \times \Delta^{14}C_F\right] \quad (1)$$

$$\delta^{13}C_{POC} = \left[f_B \times \delta^{13}C_B\right] + \left[f_S \times \delta^{13}C_S\right] + \left[f_F \times \delta^{13}C_F\right] \quad (2)$$

$$1 = f_B + f_S + f_F \quad (3)$$

We constrain end-member values using $\delta^{13}C$ and $\Delta^{14}C$ values of source-specific biomarkers in individual SPM samples. Molecular-level $\delta^{13}C$ and $\Delta^{14}C$ measurements on compounds representing known end-members allows direct assessment of the fractional contribution of the three components to river suspended POC for any specific sample independent of ancillary data. The specific compounds investigated in this study are well-established biomarkers due to their source specificity, relative diagenetic stability, and amenability for extraction and purification from geological matrices such as soils, river suspended particles and marine sediments (Eglinton and Hamilton 1967; Freeman and Colarusso 2001; Zhao et al. 2006; Galy et al. 2011). One important and inherent limitation in the approach stems from the unknown and potentially variable fractionation effects imparted on stable carbon isotope compositions to different cellular components. Differences in $\delta^{13}C$ between lipid biomarkers and bulk OM resulting from isotopic fractionation during biosynthesis, diagenesis or thermal alteration ($\delta^{13}C_{bulk} - \delta^{13}C_{lipid}$) need to be taken in account. This is especially the case for lipids, which tend to be significantly depleted in ^{13}C (5~10‰ for algae and 7~10‰ for vascular plants; 1~7‰ for petrogenic materials; Tao et al., 2015 and references therein). Since we presently have no data on $\delta^{13}C_{bulk} - \delta^{13}C_{lipid}$ offsets of typical source materials within and surrounding the Yellow River drainage basin, a moderate offset of 5 to 7‰ is applied to the measured $\delta^{13}C$ values

for each of the biomarker class used here to approximate lipid-bulk OC differences.

We have applied a random sampling (Monte Carlo, MC) computer simulation strategy to incorporate the effect of a potential spread in end-member values on the quantitative source apportionment. The MC simulations were based on the assumption that the end-member values ($\Delta^{14}C_B$, $\Delta^{14}C_S$, $\Delta^{14}C_F$, $\delta^{13}C_B$, $\delta^{13}C_S$ and $\delta^{13}C_F$) could be represented by a normal distribution, where the mean and standard deviation are estimated from measured source-specific lipid compound isotopic compositions and their measurement uncertainty. The calculations were performed using random sampling from these normal distributions, while simultaneously fulfilling Eqs. (1) to (3) and constraining the solutions to be between 1 and 0 (i.e., fractional contributions). By repeating the random sampling (4,000,000 times) and sorting the results in histograms (256 bins), distributions (as probability density functions) of the fractions f_B, f_S and f_F were obtained (Fig. S4a−S4d). These distributions were used to calculate the mean and the standard deviation as summarized in Figure 7a and Table S1. Details regarding end-member ranges are provided in the Discussion section. The MC calculations were performed in Python (Jupyter Network).

Hierarchical Cluster Analysis

In this study, the content and stable carbon isotopes of multiple compounds were determined. In order to avoid repetitive discussion, Hierarchical Cluster Analysis was used to classify various compounds into groups according to similarity of molecular characteristics (content and $\delta^{13}C_{Compound}$ values), and the Pearson correlation coefficient (R) measures the similarities between variables. The concentration matrix is standardized using

the Z-score as follows:

$$Z_{ij} = \frac{X_{ij} - \overline{X_i}}{\sigma_i}$$

Where X_{ij} is the concentration of the *i*-homolog on the *j*-sample, and X_i and σ_i are the mean and standard deviation of the *i*-homolog, respectively. For this application, the TOC normalized content and $\delta^{13}C_{Compound}$ matrixes (X($n \times m$)) with *n*-rows (the number of homologs) and *m*-columns (the number of samples analyzed) was constructed. The Pearson correlation coefficient (R) was used as a measure of the similarities between variables. The number and the structure of clusters formed using these methods are not affected with either the addition of small numbers of "bad" points or the use of a limited number of measurements.

Results

Hydrological characteristics (discharge and TSS)

Water discharge (m^3/s) and TSS (kg/m^3) were monitored on daily to monthly frequencies by the Yellow River Conservancy Commission (YRCC) (Fig. 2). The hydrological dataset was collected from the nearest hydrometric station (Lijin) to the sampling site (Shengli floating bridge, Kenli) and from Tongguan hydrometric station, which is located near the boundary of the middle and lower reaches (Fig. 1). Only limited daily TSS data are available. Water discharge and TSS exhibit large seasonal variations; the middle reach and lower reach showed broadly similar seasonal patterns but slightly different inter-annual patterns (Fig. 2). The highest water discharge at Tongguan occurred usually in September with a second smaller peak in March, while the lowest discharge occurred in May

or December–January just before the onset of summer-autumn and spring NHF periods. The maximum in TSS concentrations coincided with the timing of several NHF events over the middle reach or on the whole drainage basin scale in the wet season (e.g., August–September 2011, July–early September 2012). In addition to this peak, water discharge and TSS at Lijin shows a distinct second maximum in June–July, which is due to man-made release of turbid floodwaters from the Sanmenxia and Xiaolangdi reservoir cascades located in the front of lower reach (Fig. 1). This period of water and sediment regulation (WSR), carried out by the YRCC, usually takes place from mid-June to mid-July and is designed to induce artificial hyperpycnal flow in order to de-silt the whole lower reach below the Xiaolangdi reservoir. The lowest water discharge was recorded in February–May, and is due to sparse precipitations and extensive irrigation practices in downstream areas. The lowest TSS concentrations were observed in the dry season (November–May), likely as a consequence of weak hydrodynamic conditions and limited surface land or riverbed erosion. Based on the hydrological characteristics, the middle reach of the Yellow River is dominantly influenced by natural processes whereas the lower reach is significantly affected by both natural and man-made processes. Among different years, discharge and TSS in the lower reach during the WSR period (20 June–10 July in every year) are similar, with maxima of ~ 3500–4000 m^3/s and 12–18 kg/m^3, respectively (Fig. 2a and 2b). During the summer-autumn NHF period, discharge and TSS peak intensity and amplitude vary among different years, with stronger maxima in 2012 (Fig. 2), indicating enhanced flow and turbidity events. Over our 2-year observation period (June 2011–July 2013), total runoff ($282.5\times 10^8\ m^3$) in 2012 was 53% and 98% of that in 2011 and 2013, respectively. The corresponding sediment load (1.83

$\times 10^8$ t) was 19% and 6% higher than those in 2011 and 2013 respectively, due to the heavy and high-frequent storm events in the wet season of 2012 (Yellow River Sediment Bulletin, 2011, 2012 and 2013; http://www.yellowriver.gov.cn/nishagonggao/, accessed on 22 January 2017). Moreover, the winter season of 2012 (December 2011–February 2012) represented the first time in almost a decade that the lower reach of the Yellow River did not freeze over, resulting in higher than normal flow rates (monthly ave. max. 1160 m^3/s in December 2011; Fig. 2c).

POC characteristics

Measurements on twelve SPM samples collected from June 2011 to July 2013 were investigated in order to assess seasonal and inter-annual variations of different organic components transported by the Yellow River. Over the two-year observation period, POC concentrations (mg/L) co-varied strongly ($R = 0.98$ and 0.84; $P < 0.01$) with hydrological parameters (TSS and water discharge), with higher POC concentrations (6.97−9.41 mg/L) in the summer WSR period (June) and autumn flooding season (September) and lower values (1.56− 2.86 mg/L) during most other times of the year (Fig. 3a). Despite this variability in concentrations (ave., 4.20±2.79 mg/L), there is no systematic change in POC content normalized to TSS (POC%; 0.26–0.47 wt.%; ave., 0.34±0.07 wt.%) but a slightly higher value was observed in April (Fig. 3b). The time-series dataset also reveals only minor variability in the carbon isotopic composition of POC, with no distinct seasonal variations (Fig. 4 and 5). This isotopic consistency is reflected in both $\delta^{13}C$ values (–23.4±0.1 to –24.2±0.1‰; ave., –23.8±0.3‰) and $\Delta^{14}C$ values (−397±7 to −447±6‰; ave., −424±18‰).

Molecular abundance characteristics

Molecular distributions of three target lipid biomarkers in all twelve SPM samples exhibited similar patterns, with an even-carbon number predominance and maxima centered on *n*-C_{16} for *n*-fatty acids (*n*-FAs), an even-carbon number predominance and maxima centered on *n*-C_{28} for *n*-alkanols, and an odd-carbon number predominance centered on *n*-C_{31} for *n*-alkanes (Appendix a. Supplementary raw data). Based on the hierarchical cluster analysis of the content and stable carbon isotopes of all even-carbon-numbered *n*-FAs, *n*-alkanols and all *n*-alkanes homologs, the even-chain-length *n*-FAs were divided into three groups according to similarity of molecular characteristics: (*i*) short-chain homologs including *n*-C_{16} and *n*-C_{18} FA, (*ii*) mid-chain homologs including *n*-C_{20}, *n*-C_{22} and *n*-C_{24} FA, and (*iii*) long-chain homologs including *n*-C_{26}, *n*-C_{28} and *n*-C_{30} FA (Supplementary Fig. S1a and S2a). *n*-alkanols reveal two groups: short-chain homologs (*n*-C_{18} and *n*-C_{20} alkanols), and longer-chain homologs ($C \geq 22$ *n*-alkanols; Supplementary Fig. S1b). All odd-chain *n*-FAs and *n*-alkanols were excluded due to lower abundance and ambiguous sources. Among the *n*-alkanes, four groups were evident comprising of short-chain (incl. *n*-C_{17}), mid-chain (*n*-C_{18}–*n*-C_{25} alkanes), long-chain even (*n*-C_{26}, *n*-C_{28}, *n*-C_{30} and *n*-C_{32} alkanes), and long-chain odd (*n*-C_{27}, *n*-C_{29}, *n*-C_{31} and *n*-C_{33} alkanes) homologs (Supplementary Fig. S1c and S2b).

The concentration of short-chain compounds was uniformly low throughout the year, with the exception of a maximum during the flooding event in September 2011 (13.6, 7.44 and 0.10 μg/L for *n*-C_{16} FA, *n*-C_{18} FA and *n*-C_{17} alkane, respectively). For example, *n*-FAs

(n-C_{16}, n-C_{18}) and n-alkanes (n-C_{17}) ranged from 1.1 to 13.6 μg/L (avg., 3.1±3.4 μg/L), 0.3 to 7.4 μg/L (avg., 1.3±2 μg/L) and 0.01 to 0.10 μg/L (avg., 0.03±0.01 μg/L), respectively (Fig. 3a). In contrast, their TOC-normalized contents varied more significantly, ranging from 269 to 1446 μg/g OC (avg., 739±334 μg/g OC), 68 to 791 μg/g OC (avg., 300±208 μg/g OC) and 3 to 17 μg/g OC (avg., 8±4 μg/g OC), respectively, with higher values during low flow period and the lowest value during the WSR period (Fig. 3b).

In contrast to short-chain compounds, the concentration of long-chain plant wax derived lipid compounds co-varied more strongly with daily TSS ($R = 0.90–0.96$; $P < 0.01$) and daily water discharge ($R = 0.67– 0.74$; $P < 0.01$). For example, the summed concentration of long-chain even n-FAs ($C_{26+28+30}$), n-alkanols ($C_{24+26+28}$) and long-chain odd n-alkanes ($C_{27+29+31}$) ranged from 0.7 to 5.0 μg/L (ave., 1.8±1.2 μg/L), 0.9 to 5.6 μg/L (ave., 2.2±1.5 μg/L) and 0.6 to 2.3 μg/L (ave., 1.2±0.6 μg/L), with higher values during the high-flow WSR period and the flood events in September 2011, and lower values during those times of year characterized by lower flow (Fig. 3a). However, TOC-normalized contents of long-chain n-FAs (312 to 571 μg/g OC; ave., 442±80 μg/g OC) and n-alkanols (374 to 694 μg/g OC; ave., 539±93 μg/g OC) did not show any relationship with hydrologic parameters, but instead exhibit a distinct seasonal cycle over the two-year observation period. Specifically, higher relative abundances occurred in autumn (September-October) and during the non-WSR period in summer (June), while cold/dry seasons (November-April) and the WSR period were characterized by lower OC-normalized values (Fig. 3b). Long-chain odd n-alkanes (187 to 405 μg/g OC; ave., 316±76 μg/g OC) displayed higher values during low flow-rates (January-April) and the non-WSR period in June, but lower values during the WSR period and autumn (Fig. 3b).

Concentrations (0.1 to 0.4 μg/L; ave., 0.3±0.1 μg/L) and TOC-normalized contents (24 to 153 μg/g OC; ave., 89±48 μg/g OC) of long-chain even-carbon-numbered *n*-alkanes (i.e., C_{26}, C_{28}, C_{30}) exhibit a pattern of temporal variability that is similar to, but more variable than those of middle-chain even homologs (i.e., C_{20}, C_{22}, C_{24}; 0.05 to 0.2 μg/L; ave., 0.1±0.05 μg/L, and 13 to 114 μg/g OC; avg., 37±29 μg/g OC, respectively). Long-chain even-carbon-numbered *n*-alkane concentrations exhibited no obvious temporal patterns (Fig. 3a), but the TOC-normalized content increased from summer (June) to winter (January) and then decreased to a relatively low level by the following summer (Fig. 3b).

Molecular isotopic characteristics

Stable carbon isotope and radiocarbon ($\delta^{13}C$ and $\Delta^{14}C$) compositions of *n*-FAs and *n*-alkanes in the twelve SPM samples were also determined in this study. For short-chain compounds, $\delta^{13}C$ values ranged from –26.3±0.1 to −28.7±0.1‰ (ave., −27.5±0.8‰) and from –26.4±0.1 to −28.4±0.2‰ (ave., –27.6±0.8‰) for $\delta^{13}C_{16FA}$ and $\delta^{13}C_{18FA}$, respectively (Fig. 4a). Corresponding $\Delta^{14}C$ values ($\Delta^{14}C_{16FA}$ and $\Delta^{14}C_{18FA}$) varied from +115±10 to −85±8‰ (ave., −20±54‰) and +44±10 to −84±11‰ (ave.,–21±46‰), respectively (Fig. 5). Over the two-year observation period, short-chain *n*-FA $\delta^{13}C$ values decreased from the WSR period to autumn, and then increased to relatively high values by the following summer (Fig. 4a), while $\Delta^{14}C$ values displayed an opposite trend, increasing from WSR period to autumn and then gradually decreasing the following summer (Fig. 5). Although short-chain (C_{17}) *n*-alkane abundances exhibited the same temporal change as short-chain *n*-FAs, corresponding $\delta^{13}C$ values were more variable and generally lower, ranging from

–29.5±0.1 to –38.0±0.1‰ (ave., –33.3±2.7‰), with the lowest $\delta^{13}C$ values in autumn (October 2012) and the summer low-flow period (June 2013), and highest values in winter (January 2013) and during the summer WSR period (Fig. 4a). $\Delta^{14}C$ values of *n*-C_{17} alkane were not measured due to low abundances (Fig. 3).

For long-chain compounds, we investigated temporal variability in ^{13}C and ^{14}C isotopic compositions of plant wax-derived long-chain even-carbon-numbered *n*-FAs ($C_{26,}$ $C_{28,}$ C_{30}) and *n*-alkanols ($C_{24,}$ $C_{26,}$ C_{28}), long-chain odd- ($C_{29,}$ C_{31}) and even-carbon-numbered ($C_{26,}$ $C_{28,}$ $C_{30,}$ C_{32}) *n*-alkanes (Fig. 4b and 5). Over the two-year observation period, abundance-weighted average $\delta^{13}C_{26+28+30FAs}$ and $\Delta^{14}C_{26+28+30FAs}$ were systematically lower and less variable than corresponding short-chain FAs, ranging from −30.7±0.1 to −31.7±0.1‰ (ave., −31.3±0.3‰) and from −172±11 to −244±7‰ (ave., −208±23‰), respectively (Fig. 4b and 5). Abundance-weighted average $\Delta^{14}C_{24+26+28alkanols}$ values exhibited a similar temporal pattern with those of $\Delta^{14}C_{26+28+30FAs}$, but with slightly greater variability and less negative values (–143±10 to –243±18‰, ave., –177±32‰; Fig. 5). The $\delta^{13}C$ and $\Delta^{14}C$ values of long-chain *n*-alkanes were the lowest and exhibited the widest ranges among the three long-chain biomarker classes. Abundance-weighted average $\delta^{13}C_{29+31alkanes}$ of long-chain odd (i.e., C_{29} and C_{31}) *n*-alkanes ranged from −28.2±0.1 to −31.6±0.1‰ (ave., −30.0±1.9‰) and those ($\delta^{13}C_{even\ alkanes}$) of even *n*-alkanes (i.e., C_{26}, C_{28}, C_{30} and C_{32}) ranged from −27.0±0.1 to −30.1±0.1‰ (ave., −28.8±1.1‰) (Fig. 4b). These values were generally more variable and higher compared to those of long-chain *n*-FA. Abundance-weighted average $\Delta^{14}C_{29+31alkanes}$ and $\Delta^{14}C_{even\ alkanes}$ values, which varied from −288±10 to −612±9‰ (ave., –469±94‰), and from −700±40 to –961±21‰ (ave., –858±

99‰), respectively (Fig. 5), were also more variable and markedly lower than those of corresponding long-chain *n*-FAs and *n*-alkanols. Over the observation period, cold and dry seasons (November to April) always corresponded to higher $\delta^{13}C$ and lower $\Delta^{14}C$ values for long-chain *n*-alkanes, while warm and wet seasons (June to October) corresponded to lower $\delta^{13}C$ and higher $\Delta^{14}C$ values. Long-chain even-carbon number (i.e., C_{26}, C_{28}, C_{30} and C_{32}) *n*-alkanes were most strongly ^{14}C-depleted, especially during winter and spring time (Fig. 5).

For lignin derived phenols, the abundance-weighted average $\Delta^{14}C$ values of syringyl and vanillyl phenol $\Delta^{14}C_{V+S\ phenols}$ exhibited strong temporal variability (1σ = 65‰), with the highest value (+21±8‰) in summer (June) and the lowest value (–132±36‰) in winter (January). Lignin phenol $\Delta^{14}C$ values were generally higher than those of plant wax derived long-chain lipid biomarkers from corresponding SPM samples (Fig. 5).

Discussion

Molecular isotopic insights into temporal variability in POC sources

In this study, we undertake a detailed examination of temporal variations in carbon isotopic compositions of POC and of source-specific biomarkers. Yellow River POC $\delta^{13}C$ values (–23.4 to –24.2‰; Fig. 4a) are relatively high compared to those draining watersheds dominated by C_3 vegetation (Raymond and Bauer 2001; Zou et al. 2006; Martin et al. 2013; Bouchez et al. 2014). C_4-dominanted vegetation and heterotrophic aquatic organisms, especially near wetlands and reservoirs, along the lower Yellow River may be responsible for inputs of ^{13}C-enriched OC input (Fig. 6). The relatively depleted ^{14}C content and corresponding old radiocarbon age (4000–4690 ^{14}C yr; Fig. 5) may reflect large

contributions from relict floodplain soil sediments, heavily weathered loess deposits or old sedimentary rock inputs (Keil et al. 1997; Wu et al. 2005; Wang et al. 2012; Tao et al. 2015). As shown in Figure 4 and 5, standard deviations (1σ) of POC isotopic characteristics of samples spanning different seasons fall within threefold analytical error. Despite this invariance in POC ^{13}C and ^{14}C contents, distinct isotopic variability is apparent at the molecular level (Fig. 6), implying that OC inputs and dynamics are more complex and variable than apparent at the bulk level. We therefore further examine molecular isotopic signals in order to derive insights into intrinsic temporal variability in Yellow River suspended POC.

Isotopic compositions of molecular markers provide a window into the specific source inputs contributing to the overall (bulk) OC signature, and provide a valuable approach for quantitative apportionment of OC sources. Although there are intrinsic uncertainties in the isotope mass balance approach, these uncertainties are sharply reduced when multiple lines of molecular (isotopic) evidence converge on similar end-member values. We consider, therefore, that this approach provides a crucial means to track different OC sources to highly complex bulk OM pools (e.g., riverine POC), and to assess temporal variability in source inputs.

Contemporary/modern biomass OC

Short-chain (C_{16} and C_{18}) *n*-FAs are ubiquitous molecular marker compounds that are abundant in terrestrial plant leaf tissue, aquatic biomass and soil OM (Chikaraishi and Naraoka 2006; Volkman et al. 2008). In the Yellow River, relatively high

abundance-weighted average $\Delta^{14}C$ values of C_{16} and C_{18} *n*-FAs ($\Delta^{14}C_{16+18FA}$: +44‰ to −85‰, ave., −20‰) imply an origin from a relatively labile and fast turnover (decades) biogenic material pool that is only slightly lower than $\Delta^{14}C$ of atmospheric CO_2.

In order to distinguish and examine temporal variability in contributions from different biogenic sources, short-chain *n*-FA characteristics were compared with those of *n*-C_{17} alkane - an aquatic biomarker (Gelpi et al. 1970; Collister et al. 1994a) with very low $\delta^{13}C$ values (as low as −38.0‰; Fig. 4a). Temporal variability in $\delta^{13}C$ values of this marker should therefore be tightly coupled with the abundance and isotopic composition of dissolved inorganic carbon (DIC) due to photosynthesis and carbon fixation. The *n*-C_{17} alkane is most ^{13}C-depleted in autumn and during the low flow summer period, with higher $\delta^{13}C$ values in winter and during the WSR period (Fig. 4a). This trend is consistent with higher concentrations and a more ^{13}C-depleted DIC signature in autumn as a consequence of organic matter decomposition and also terrestrially-derived groundwater DIC inputs (Hotchkiss et al. 2015), while more ^{13}C-enriched DIC signals stem from dissolution of carbonate and siliciclastic rocks during weathering reactions in spring and winter (Wang et al. 2016). The pattern of seasonal variability in $\delta^{13}C$ of short-chain *n*-FA is similar to that of the *n*-C_{17} alkane ($\delta^{13}C_{17alkane}$), albeit lower in amplitude (Fig. 4a). Although there are only two data point available for $\Delta^{14}C_{DIC}$ in the Yellow River (Wang et al. 2016), higher $\Delta^{14}C_{16+18FA}$ values (−2‰) and $\Delta^{14}C_{DIC}$ values (−125‰) were observed in October, while lower $\Delta^{14}C_{16+18FA}$ values (−50‰) and $\Delta^{14}C_{DIC}$ values (−164‰) were evident in Spring (April). These parallel time-series variations suggest that aquatic production is likely a source of short-chain *n*-FAs, and hence corresponding carbon isotopic compositions of

short-chain *n*-FAs echoes that of aquatic biomass produced via photosynthetic DIC fixation.

However, ^{14}C signals of short-chain *n*-FAs are consistently ca. 110−120‰ higher than that of Yellow River DIC, indicating that the former partly derive from fresh vascular plant carbon or heterotrophic organisms that utilize a different carbon source (e.g., fresh terrestrial plant detritus). As evident from Figure 6, $\delta^{13}C_{16+18FA}$ values are also consistently 1.9− 9.5‰ higher than that of aquatic lipid biomarker (*n*-C_{17} alkane), indicating ^{13}C-enriched (e.g., C_4-dominanted vegetation and heterotrophic aquatic organisms) sources could partly contribute short-chain *n*-FAs in the Yellow River.

Short-chain *n*-FAs are also prevalent in soils (Otto and Simpson 2005; Chikaraishi and Naraoka 2006). In order to estimate potential contributions from the soil end member, short-chain *n*-FA isotopic characteristics were compared with those of a well-established suite of terrestrial plant biomarkers – lignin phenols. Lignin has been proposed to be primarily supplied to rivers via surface export (run-off) of fresh, younger plant-derived (detritus, litter) or surface soil OC (Feng et al. 2013b; Martin et al. 2013). In the Yellow River, lignin-derived phenols from the same samples exhibited younger ages in summer and autumn and older ages in winter and spring (Fig. 5), which is consistent with more plant growth in warm and wet seasons relative to cold and dry seasons. Erosion from less-vegetated land surfaces, particularly in cold and dry seasons, would promote mobilization of older plant markers (plant wax lipids, lignin phenols) from surface and deeper soil layers. Given that the temporal variability in $\Delta^{14}C$ values of short-chain *n*-FAs does not parallel that of lignin−derived phenols (i.e., ^{14}C ages short-chain *n*-FAs do not

increase in winter; Fig. 5), we therefore infer that contributions of aged (mineral soil-derived) short-chain n-FAs are insignificant compared to those from fresh plant-derived and aquatic sources. Accordingly, we interpret short-chain *n*-FAs exported by the Yellow River SPM as reflecting fresh biogenic contributions from both ^{13}C-enriched (e.g., C_4-dominanted vegetation and heterotrophic aquatic organisms), and ^{13}C-depleted (e.g., aquatic primary production and/or C_3 plants) sources (Fig. 6). Therefore, their carbon isotopic compositions are considered representative of isotopic end-member values for overall OC derived from contemporary/modern biomass inputs to the Yellow River.

For a quantitative estimation, a three end-member isotopic approach was applied to assess the relative contribution of *n*-$C_{16,18}$ FAs derived from aquatic production ($f_{aquatic}$), vascular C_3 plants (f_{C3}) and vascular C_4 plants (f_{C4}), in SPM from two different time intervals (October and April). $\delta^{13}C_{aquatic}$, $\delta^{13}C_{C3}$, $\delta^{13}C_{C4}$ and $\Delta^{14}C_{aquatic}$, $\Delta^{14}C_{C3}$, $\Delta^{14}C_{C4}$ are corresponding end-member isotopic compositions of individual sources, respectively. The MC simulation (see method) was used to account for variability in the end-member values in the source apportionment calculation.

$$\Delta^{14}C_B = \left[f_{aquatic} \times \Delta^{14}C_{aquatic} \right] + \left[f_{C_3} \times \Delta^{14}C_{C_3} \right] + \left[f_{C_4} \times \Delta^{14}C_{C_4} \right]$$

$$\delta^{13}C_B = \left[f_{aquatic} \times \delta^{13}C_{aquatic} \right] + \left[f_{C_3} \times \delta^{13}C_{C_3} \right] + \left[f_{C_4} \times \delta^{13}C_{C_4} \right]$$

$$1 = f_{aquatic} + f_{C_3} + f_{C_4}$$

We defined $\delta^{13}C_{16+18FAs}$ and $\Delta^{14}C_{16+18FAs}$ as isotopic representatives of contemporary biomass inputs ($\delta^{13}C_B$ and $\Delta^{14}C_B$). We used literature $\Delta^{14}C_{DIC}$ values (-125 ± 2.1‰ in October; -164 ± 2.1‰ in April) and $\delta^{13}C$ values (-32.7 ± 0.1‰ in October; -30.9 ± 0.1‰

512 in April) of typical aquatic lipid biomarkers (*n*-C_{17} alkane) for the aquatic autotrophic (and
513 associated heterotrophic) end-member. Based on literature data for the stable carbon
514 isotopic composition of plant wax-derived *n*-alkanes (Collister et al. 1994b; Freeman and
515 Colarusso 2001) and considering ~2‰ ^{13}C-depletion for corresponding *n*-FAs relative to
516 *n*-alkanes (Wiesenberg et al. 2004), we assumed a fixed $\Delta^{14}C$ and $\delta^{13}C$ values of +50±10‰
517 and –32.8±2.4‰ for recently-synthesized higher C_3 plant-sourced *n*-$C_{16,18}$ FAs, and +50±
518 50‰ and –20.6±2.1‰ for higher C_4 plant-sourced *n*-$C_{16,18}$ FAs, respectively. In these two
519 SPM samples, the fraction of contemporary biomass-sourced organic compounds in
520 October and April, taking *n*-$C_{16,18}$ FAs as an example (Table 2). Short-chain *n*-FAs (and
521 associated contemporary/modern biomass OC) in the lower reach of the Yellow River stem
522 from at least three sources, and includes a significant proportion of C_4 higher plant and
523 aquatic sources despite the dominance of C_3 vegetation in the upper and middle reaches of
524 the Yellow River. The proportion of recently-fixed higher plant input was predominant in
525 October (71%), which is consistent with strong surface terrestrial material erosion during
526 the autumn NHF period. Zhang et al. (2010) reported vegetation coverage in the Yellow
527 River drainage basin, indicating that C_3 vegetation predominates in higher altitude regions
528 of upper and middle reaches whereas contributions of C_4 vegetation generally increases
529 with decreasing elevation towards the lower basin. In some regions of the lower part of the
530 river basin, especially near wetlands and reservoirs, C_4 vegetation contribution can reach up
531 to 50%. From the MC source apportionment of contemporary biomass OC, the greater C_3
532 plant contribution to Yellow River SPM in October (31±10%) than in April (13±6%)
533 may reflect intensified erosion of surface land during the autumn NHF period that promotes

mobilization of C_3 plant tissue from the upper to the lower reach. Notably, however, ~40% of the contemporary biomass organic component originated from C_4 plant sources. The relative constancy of this proportion during different sampling times implies that contemporary C_4 plant biomass inputs are local, and independent of temporal variations in hydrodynamic processes associated with physical erosion or transportation. In addition, fractional contributions from aquatic sources to the overall contemporary biomass-derived organic component tended to be higher in April (46%) under conditions of low flow where light limitation is alleviated due to lower turbidity. While aquatic primary production is unlikely to be prominent in such a turbid river, there could certainly be secondary (heterotrophic) aquatic productivity fueled by supply of fresh carbon from the surrounding landscape. In this case, light availability would not be an issue. However, it is important to point out that although aquatic production comprises a major source for *n*-$C_{16, 18}$ FAs and associated contemporary biomass-derived OC, this does not mean that aquatic production is a major source for bulk OC. In fact, results from the three end-member mixing model suggest that contemporary biomass OC - including aquatic production and freshly synthesized terrestrial plant detritus - accounts for a relatively minor component (13−22%) of bulk POC in this turbid river system (see discussion below; Fig. 7a).

Soil OC

Approximately 88% of the sediment load of the Yellow River originates from the Loess Plateau (Wang et al. 2011; Hu et al. 2012b), and corresponding loess/soil-derived OC likely comprises a substantial fraction of the OC discharged to the and buried in the, adjacent Chinese marginal seas. Plant wax *n*-alkyl lipids and lignin-derived phenols are two

557 well-established groups of biomarker compounds of terrestrial plant biomass which have
558 been widely applied to trace the fate of vascular plant-derived OC in soils and fluvial
559 systems (e.g., Feng et al. 2013; Martin et al. 2013). Gustafsson et al. (2011) performed
560 compound-specific ^{14}C analysis of plant wax *n*-alkyl lipids (FAs and alkanes) in
561 river-dominated Siberian margin sediments and concluded that the distinct old OC ^{14}C ages
562 is consistent with supply from deeper layers of Arctic soils. In this study, we also consider
563 ^{14}C and ^{13}C-depleted (pre-aged) plant wax FAs and alkanols (Fig. 6; i.e., *n*-$C_{26, 28, 30}$ FAs,
564 *n*-$C_{24, 26, 28}$ alkanols) as isotopically representative of bulk pre-aged soil OC, and use these
565 signatures to track temporal variability in pre-aged mineral-bound soil OC contiributions to
566 Yellow River SPM.
567 As shown in Figure 4b and 5, ^{13}C and ^{14}C isotopic characteristics of *n*-$C_{26+28+30}$ FAs and
568 *n*-$C_{24+26+28}$ alkanols exhibit minor temporal variability, with 1σ values (0.3‰ for $\delta^{13}C$ and
569 27‰ for $\Delta^{14}C$, respectively) falling within measurement uncertainty (0.2‰ and 40‰,
570 respectively; see experiment methods). Furthermore, their carbon isotopic compositions and
571 OC-normalized concentrations do not co-vary with TSS or water discharge (Fig. 3b and
572 Fig. S3a− S3d). Both of these observations imply relatively constant soil organic matter
573 contributions to the Yellow River POC. Furthermore, the uniform isotopic compositions
574 suggest a common origin for plant wax lipids and associated pre-aged soil OC irrespective
575 of hydrological regime. Any type of erosion, especially deep mobilization process such as
576 transport via underground conduits, gully erosion or occasional mudslides, seems to
577 transfer pre-aged soil/loess OC from the Loess Plateau to the Yellow Rive system.
578 In contrast, ^{14}C characteristics of lignin-derived phenols exhibit greater seasonality. In
579 the Yellow River SPM, lignin phenol ^{14}C ages are younger in warm and wet seasons

(summer and autumn; Fig. 5), indicating more rapid mobilization of surface soil OC and greater inputs of fresh terrestrial primary production via relatively high run-off (Fig. 2a and 2c). However, lignin-derived phenols generally become older in the dry and cold seasons with values closer to *n*-alkyl long-chain lipids (Fig. 5). This suggests pre-aged mineral-bound lignin are proportionally greater in cooler and less extensively vegetated conditions, and both plant-derived organic compounds (lignin derived phenols and *n*-alkyl lipids) more strongly reflect re-mobilization of deeper mineral-bound soil OC during winter and early spring time. The ^{14}C contents of lignin-derived phenols also weakly correlate with hydrological parameters, as the proportion of fresh (^{14}C-enriched) phenols increases with increasing turbidity and flow rate (Fig. S3g and S3h). We concluded that hydrologic conditions seasonally influence contributions of fresh higher plant-derived detritus OC via rapid surface export (run-off), while both the proportion and isotopic characteristics of the predominant pre-aged soil OC component remains relatively invariant. Overall, these findings imply that different terrestrially-derived organic compounds may exhibit temporal variability due to contrasting stabilization, mobilization and transport processes within the river basin.

Fossil/petrogenic OC

Although long-chain odd-carbon-numbered *n*-alkanes (i.e., C_{29+31}) are frequently-used biomolecular tracers of vascular plant-derived carbon (Eglinton and Hamilton 1967; Collister et al. 1992; Collister et al. 1994b), their distributions in contemporary soils and sediments may be influenced by petrogenic and anthropogenic hydrocarbon inputs (Pearson and Eglinton 2000; Drenzek et al. 2007; Kusch et al. 2010). In the Yellow River,

abundance-weighted average $\delta^{13}C$ values of long-chain odd *n*-C_{29+31} alkanes display distinct seasonal variability (1σ = 1.1‰), with the lowest values (min. –31.6‰) in wet and warm seasons (autumn and summer) and higher values (max., –28.2‰) in dry and cold seasons (winter and spring) (Fig. 4b). The seasonal growth pattern of C_4/C_3 vegetation along the Yellow River drainage cannot readily explain this more ^{13}C-enriched signal of *n*-C_{29+31} alkanes in cold seasons. However, sedimentary rock outcrops and numerous coal mines in upper and middle sections of the drainage basin may serve as an additional source of ^{13}C-enriched *n*-alkanes (Wiesenberg et al. 2004; Jia and Peng 2005; Tao et al. 2015), with proportionally greater contributions in winter and spring (Wang et al. 2016). Corresponding ^{14}C data also support this interpretation: *n*-C_{29+31} alkanes exhibit older ^{14}C ages (2670 to 7550 yr) compared to those of *n*-$C_{26+28+30}$ FAs and *n*-$C_{24+26+28}$ alkanols, with the oldest ^{14}C ages in cold seasons (Fig. 5), consistent with fossil inputs. We therefore attribute the large temporal variation in $\Delta^{14}C$ values of *n*-alkanes to variable fossil hydrocarbon contributions, with higher proportions during cold seasons when terrestrial primary productivity is low. Long-chain even-carbon-numbered *n*-alkanes (i.e., $C_{26+28+30+32}$) show similar seasonal variability in carbon isotopic composition to the *n*-C_{29+31} alkanes, but with more significant ^{13}C-enrichment and ^{14}C-depletion (Fig. 4b and 5). In particular, $\Delta^{14}C$ values of *n*-$C_{26+28+30+32}$ alkanes from cold season samples range from –934 to –961‰ (Fig. 5), indicating an almost exclusive origin from fossil sources. However, the biospheric contribution of *n*-$C_{26+28+30+32}$ alkanes increases in warm seasons with relatively ^{13}C−depleted and ^{14}C−enriched signals.

In contrast to plant wax FAs and alkanols, hydrologic influence on long-chain

625 *n*-alkanes manifests itself in their carbon isotopic compositions in a manner similar to that
626 of lignin-derived phenols. Specifically, parallel isotopic variability is evident in long-chain
627 *n*-C_{29+31} alkanes and *n*-$C_{26+28+30+32}$ alkanes when the proportion of plant-derived *n*-alkanes
628 (characterized by ^{13}C-depletion and ^{14}C-enrichment) increases with increasing turbidity and
629 flow rate (Fig. S3e, S3f, S3i and S3j). Feng et al (2013b) measured ^{14}C contents of
630 lignin-derived phenols and plant wax lipids in a suite fluvially-dominated Arctic sediment
631 samples, and found that plant wax *n*-alkanes and lignin-derived phenols both carried a
632 strong plant debris ^{14}C signal whereas plant wax FAs did not. Overall, long-chain *n*-alkanes
633 appear to derive from multiple sources, including plant detritus, mineral soils/loess and
634 fossil materials. The seasonality of the former source can be attributed to temporal
635 variability in carbon isotopic compositions of long-chain *n*-alkanes. Notablely, carbon
636 isotopic characteristics of long-chain even-carbon-numbered *n*-alkanes in colder and low
637 flow periods show a predominant petrogenic signal with minor influence from plant detritus,
638 and provide a window into the isotopic characteristics of petrogenically-sourced OC
639 contributing to the bulk POC signal.
640
641 **Temporal variations in OC component fluxes**
642 Over the observation period, the composition and isotope characteristics of bulk OC in
643 the Yellow River SPM remained relatively invariant despite significant variability in
644 sediment and water flux. However, distinct variations in molecular isotopic characteristics
645 were evident, and these can be used to gain insights into the dynamics of specific OC
646 components contributing to the suspended load. A three end-member mixing model based
647 on the $\delta^{13}C$ and $\Delta^{14}C$ values of bulk and source-specific biomarkers is used here to estimate

seasonal variations in the relative fractional proportions of contemporary/modern biomass (f_B), pre-aged soil (f_S), and fossil (f_F) OC (see method; and more details in Tao et al., 2015).

Based on the source assignments discussed above, we constrain end-member values using $\delta^{13}C$ and $\Delta^{14}C$ values of corresponding source-specific biomarkers in each sample (the black triangle in Fig. 6). The abundance-weighted average carbon isotopic composition of *n*-$C_{16,18}$ FAs were to define contemporary biomass end-member values ($\Delta^{14}C_B$, $\delta^{13}C_B$), with $\delta^{13}C$ values of −22.61 to −20.46‰ (+6‰ corrected after $\delta^{13}C_{bulk} - \delta^{13}C_{biogenic\ lipid}$ fractionation) and standard deviation of 1.00 to 1.03‰, and $\Delta^{14}C$ values of −83 to +85‰ and standard deviation of 6 to 9‰). The abundance-weighted average carbon isotopic composition of long-chain fatty acids (*n*-$C_{26,28,30}$ FAs) were selected as the pre-aged soil end member ($\Delta^{14}C_S$, $\delta^{13}C_S$), with $\delta^{13}C$ values of −25.72 to −24.72‰ (+6‰ corrected after $\delta^{13}C_{bulk} - \delta^{13}C_{biogenic\ lipid}$ fractionation) and standard deviation of 1.00 to 1.02‰, and $\Delta^{14}C$ of −244 to −172‰ and standard deviation of 7 to 14‰. We assign $\Delta^{14}C_F$ as −1000‰ and $\delta^{13}C_F$ as the abundance-weighted average $\delta^{13}C$ value (−28.0‰) of even-carbon-numbered *n*-alkanes ($C_{26,28,30,32}$) in cold seasons when they show extremely low ^{14}C content <920‰), with standard deviation of 1.07‰ for $\delta^{13}C_F$ and with standard deviation of 21‰ for $\Delta^{14}C$. Standard deviation of end-member $\Delta^{14}C$ values only include measurement uncertainty for compound-specific ^{14}C analysis, while standard deviation of end-member $\delta^{13}C$ values consist of measurement uncertainty for compound-specific ^{13}C analysis and ±1‰ spread due to 5−7‰ correction for $\delta^{13}C_{bulk}$–$\delta^{13}C_{lipid}$ fractionation.

Figure 7a shows average values of all possible solutions derived from three end-member mixing model calculations, and reveals the temporal variability in fractional

proportions of contemporary biomass, pre-aged soil and fossil OC (f_B, f_S, and f_F, respectively) in Yellow River SPM. Error bars represent standard deviations of all possible solutions estimated via the MC simulation strategy for source apportionment calculations incorporating uncertainties in end-member values (Fig. S4). Over the investigation period, we find that Yellow River POC comprises 13±8% to 22±13% contemporary biomass OC, 44±15% to 57±11% pre-aged soil OC, and 29±2% to 35±3% fossil OC (Table S1). f_B is high in summer and autumn, likely reflecting elevated productivity and surface runoff due to high precipitation during wet and warm summer seasons (June to October), and dead leaf fall in autumn, respectively. Moreover, higher temperatures and lower turbidity in upstream tributaries/reservoir would promote high biogenic productivity (Liu et al. 2003; Gong et al. 2006; Wang et al. 2010), as well as to increase aquatic secondary (heterotrophic) productivity fueled by supply of fresh carbon from the surrounding landscape downstream. The lowest f_B values occurred in winter and spring, suggesting relatively weak surface erosion during low flow periods. In contrast, f_S is high in winter and spring (December to April), implying different mechanisms of supply of loess/mineral soil supply to the river. Thus, whereas variations in f_B imply surficial pools of terrestrial OC (traced by short-chain FAs) increase during high flow conditions, deeper-sourced OC materials, including mineral soil/loess OC (long-chain *n*-FAs and *n*-alkanols) and fossil OC (even-carbon-numbered *n*-alkanes) reflect more constant base flow conditions (Sanderman et al. 2009). Temporal variations in f_S may thus reflect processes intrinsic to the source region, such as preferential mobilization of deeper soils and pre-aged OC relative to fresh vegetation cover. Alternatively, mobilization processes associated with ice- and snow-melt may increase

692 pre-aged soil OC (f_S) export in winter and spring. Finally, f_F is relatively uniform with only
693 slightly elevated proportions during wet and warm seasons (Fig. 7a). The latter may reflect
694 resuspension of higher-density petrogenic materials (e.g., rock debris) along the main
695 stream by intensive riverbed scouring/erosion processes (Galy et al. 2015) during autumn
696 NHF and WSR period. In summary, our findings indicate that hydrologic conditions exert
697 an influence on the proportional contributions of petrogenic and especially fresh
698 plant-derived OC, while the proportion and isotopic characteristics of the predominant
699 pre-aged soil OC component remain relatively insensitive to variations in TSS and
700 discharge.

701 Our sampling site is near the last hydrological station (Lijin) of the Yellow River, ~50
702 km upstream from the estuary. Thus, POC flux at this location likely reflects overall fluvial
703 POC supply to the adjacent marginal seas. Since 1855, a modern Yellow River delta formed
704 at the interface between the river and the adjacent marginal sea, along with total land
705 expansion of 2849 km^2 till to the present. From 2000 to 2007, the delta experienced erosion
706 due to the decrease of sediment load in the lower Yellow River and the delta region (Peng et
707 al. 2010). Annually, modern Yellow River sediment export accounts for ~70% of annual
708 sediment burial in the Bohai & Yellow Sea (Tao et al. 2016 and references therein). Thus,
709 understanding the variations in the flux and composition of exported fluvial material is
710 essential for prediction of the future evolution of this marginal sea system, and likely for
711 other river-dominated margins. Combining estimates of the monthly suspended sediment
712 flux at Lijin station (Table 3, Yellow River Sediment Bulletin, 2011, 2012 and 2013) and
713 our isotopic mass balance estimates, we calculate a seasonal supply budget for the three
714 different OC components to the Chinese marginal seas (Fig. 7b). Although temporal

variability in fractional contributions is very small for each component contributing to bulk POC (Fig. 7a), fluxes of each component show large temporal variability, peaking in September and June, synchronous with the autumn flood event and WSR episodes, respectively (Fig. 7b). These temporal variations imply that typical strong seasonality in rainfall, extreme climate events and human activity (water and sediment regulation) can all significantly influence fluvial OC export from the Yellow River to the adjacent Chinese marginal seas. As expected, monthly fluxes of TSS and the three different OC components exhibit significant correlations with monthly discharge, Q (Fig. 8). Since the latter is monitored almost monthly, these correlations imply that fluxes for the three different OC components can be extrapolated to periods when OC information is unavailable, thereby reducing the uncertainty introduced by relatively low sampling frequency, in particular during high flow events. Our calculations indicate large monthly variations in Yellow River delivered OC to the adjacent Bohai/Yellow Sea, ranging between 0.03±0.42 to 3.58±2.99 × 10^4 t/month of contemporary OC, 0.15±1.33 to 10.62±9.33 × 10^4 t/month of pre-aged soil OC, and 0.08±0.87 to 6.43±6.02 × 10^4 t/month of fossil OC (Table 3).

We calculate that 6.1±3.2 × 10^4 t/yr and 10.2±4.8 × 10^4 t/yr, 17.1±6.4 × 10^4 t/yr and 29.7±14.4 × 10^4 t/yr, 11.1±9.9× 10^4 t/yr and 18.24±15.0 × 10^4 t/yr of modern biomass derived, pre-aged soil derived and fossil OC was exported to the Chinese marginal seas for different study years, respectively (Table 3). Our calculated POC fluxes for the second year of our study (0.581±0.213 Mt/yr) are 70% greater than those in the first year of our study (0.343±0.122 Mt/yr), consistent with heavier and more high-frequent storm events during the wet season (June to September) of 2012 compared to 2011 (Fig. 2; Yellow River

737 Sediment Bulletin, 2011, 2012 and 2013). These values are broadly similar to other recent
738 estimates of annual POC flux (0.389 Mt/yr from 2009, Wang et al., 2012; 0.41 Mt/yr from
739 July 2011 to June 2012, Ran et al., 2013). Taking the month of July as an example, pre-aged
740 and fossil OC fluxes in 2012 are about 4.5 times as large as those in 2011, consistent with
741 early arrival of intense precipitation and the occurrence of a basin-scale flood event in July,
742 2012.

743 Overall, natural and human-induced variations in discharge and TSS strongly
744 influence the flux but not the composition of POC exported by the modern Yellow River.
745 Pre-aged soil OC consistently represents the major component irrespective of hydrologic
746 and hydrodynamic conditions. The annual POC export by the Yellow River corresponds to
747 less than 1% of global POC flux to global oceans. However, the very high burial efficiency
748 of pre-aged soil and fossil OC in the adjacent Chinese marginal seas (up to 100% and 70%,
749 respectively; (Tao et al. 2016) implies that Yellow River represents a significant source of
750 non-modern terrestrial OC to marine sediments, with extreme climate events (e.g, floods)
751 modulating transport of this old OC from the continent into the sea.

752

753 **Comparison of the OC composition of the Yellow River with other major world rivers**

754 Despite its extremely high sediment load, the POC flux (0.344–0.584 Mt/yr) of the
755 Yellow River is relatively low as a result of significantly lower POC content (0.26–0.47%)
756 than the global mean (0.95%; with mean per river flux of 2.833–4.651 Mt/yr calculated
757 based on 60-river dataset from Ludwig et al., 1996 and 43-river dataset from Galy et al.,
758 2015). Nevertheless, the predominance of refractory and pre-aged OC (~80%) from
759 loess/mineral soil deposits results in burial of significant amounts of old OC in adjacent

margin sediments. However, an unusual characteristic of the Yellow River is the temporal uniformity in the carbon isotopic composition of POC (Fig. 9), and several other rivers show marked seasonal variability in the proportions of different sourced OC as estimated by two end-member or three end-member models (Raymond et al. 2004; Hossler and Bauer 2012; Martin et al. 2013; Lamoureux and Lafrenière 2014). Although time-series studies of radiocarbon characteristics fluvial POC remain rare and those reported are generally insufficient to capture seasonal or inter-annual OC cycles, some comparisons can be drawn from the limited ^{14}C dataset shown in Figure 9, For example, large tropical rivers, such as the Amazon and Mekong, are also characterized by high sediment load, and exhibited significant temporal variability in $\Delta^{14}C$ values of exported POC when compared to our observations from the Yellow River. This may be a consequence of greater and more variable proportions of young biospheric OC exported from the watershed and floodplain in response to seasonal (monsoon) rainfall patterns (Martin et al. 2013; Moreira-Turcq et al. 2013). POC ^{14}C characteristics in non-monsoon rivers such as Hudson, Parker, York draining the northeastern USA, may be primarily influenced by seasonal variations in OC fluxes from river aquatic productivity (Raymond and Bauer 2001; Hossler and Bauer 2012). In high latitude regions, such as the Arctic rivers (West River and East River), highly seasonal permafrost thaw and plant growth likely influence the composition and age of POC transported by streams and rivers (Lamoureux and Lafrenière 2014). Moreover, small high mountainous rivers, such as Lanyang His (Taiwan) and Narayani (a tributary of Ganges), tend to carry more variable and greater proportions of ^{14}C-free petrogenic POC via sedimentary rock erosion, which is strongly influenced by seasonal changes in precipitation and surface run-off (Kao and Liu 1996).

In addition to the Yellow River, relatively constant POC ^{14}C compositions have been found in some other fluvial systems, especially the large Asian rivers originating from the Qinghai-Tibet Plateau (Brahmaputra, Ganges and Changjiang; Fig. 9). This may reflect substantial soil OC contributions from cold, semi-arid and scarcely vegetated areas north of the Himalayan range or the Chinese Loess Plateau. Alternatively, homogeneous compositions may be a product of modification of fluvial POC during long-distance river transport. Meanwhile, a predominant input of pre-aged permafrost soil from a highly disturbed Arctic watershed (Ptarmigan; Fig. 9) has also been suggested as an explanation for the lack of temporal variability in ^{14}C composition of fluvial POC (Lamoureux and Lafrenière 2014). Figure 5 shows that time-series variations (trend and amplitude) in Yellow River bulk POC ^{14}C compositions generally co-varied with that of the plant wax biomarkers (n-$C_{26+28+30}$ FAs). As previously mentioned, we consider the latter as tracers for pre-aged mineral-bound soil inputs, which display a narrow temporal change. The relatively invariant composition of Yellow River POC is thus attributed to the high proportion of SPM in the Yellow River derived from the loess deposits, a phenomenon that is analogous to permafrost-dominated watersheds in polar region. The OC homogeneity in these pre-aged mineral soil-dominated watersheds facilitates robust predictions in terms of OC transport dynamics. It also provides a relatively stable benchmark against which to compare compositions of such river systems in the past (sediment cores) and in the future.

Conclusions

An investigation of Yellow River SPM collected over a 2-year period revealed relatively invariant bulk OC characteristics, while the carbon isotopic characteristics of

source-specific biomarkers indicate that the OC is inherently heterogeneous. At least three source components are distinguished that exhibit distinct and systematic temporal variation in proportional abundance and composition: (*i*) contemporary sources (aquatic OC, surface detrital terrestrial plant OC), influenced by aquatic production, plant phenology and hydrological conditions, (*ii*) pre-aged terrestrial sources (mineral-bound OC derived from loess/soil deposits), influenced by deep soil mobilization processes that are largely independent of hydrodynamics and surface runoff, and (*iii*) fossil OC (derived from petrogenic sources and fossil fuels), influenced by erosion of sedimentary rocks or anthropogenic processes.

Application of a mixing model based on bulk and molecular isotopic ($\delta^{13}C$ and $\Delta^{14}C$) signatures revealed that the Yellow River POC composition exhibits minor temporal variability on both seasonal and inter-annual scales despite dramatic changes in TSS and discharge. While changes in overall flux of each source component is dominated by seasonally varying hydrological conditions (especially TSS), constancy in composition of fluvial OC was linked to a predominant input of the homogeneous loess/soil OC.

Variations in fractional contributions of the three different OC components have significant implications for regional scale carbon cycling given their different connection to atmospheric reservoirs and fates (i.e., remineralization vs burial efficiency). Both natural and human modulation of hydrological conditions exerts dominant control on fluxes of all three components in the Yellow River. Moreover, the consistent relationships that emerge between OC composition and seasonally varying fluvial dynamics provide a means to reconstruct past and predict future changes in the flux and nature of OC discharge from the river. In this context, a key facet of the biomarker [isotope] approach is the ability to trace

OC signatures into the sedimentary record, where they provide one of the key tools for paleoclimate and paleoenvironmental reconstruction. Such records are frequently targeted in land-proximal marine sedimentary sequences where interpretation of bulk OC signatures is confounded by contributions from marine productivity. Thus, understanding [temporal] variability of the amount and isotope characteristics of specific organic compounds is important not only in the context of understanding source-to-sink carbon dynamics, but also for more informed interpretation of down-core records.

References

Aller, R. C., and N. E. Blair. 2004. Early diagenetic remineralization of sedimentary organic C in the Gulf of Papua deltaic complex (Papua New Guinea): Net loss of terrestrial C and diagenetic fractionation of C isotopes. Geochim. Cosmochim. Acta **68:** 1815–1825.

Aller, R. C., N. E. Blair, and G. J. Brunskill. 2008. Early diagenetic cycling, incineration, and burial of sedimentary organic carbon in the central Gulf of Papua (Papua New Guinea). J. Geophys. Res.: Earth Surface **113:** 2156–2202.

An, Z. 2000. The history and variability of the East Asian paleomonsoon climate. Quat. Sci. Rev. **19:** 171–187.

Battin, T. J., S. Luyssaert, L. A. Kaplan, A. K. Aufdenkampe, A. Richter, and L. J. Tranvik. 2009. The boundless carbon cycle. Nat. Geosci. **2:** 598–600.

Berner, R. A. 1982. Burial of organic carbon and pyrite sulfur in the modern ocean: its geochemical and environmental significance. Am. J. Sci. **282:** 451–473.

Bianchi, T. S. 2011. The role of terrestrially derived organic carbon in the coastal ocean: A changing paradigm and the priming effect. Proc. Natl. Acad. Sci. **108:** 19473–19481.

Blair, N. E., and R. C. Aller. 2012. The fate of terrestrial organic carbon in the marine environment. Annu. Rev. Mar. Sci. **4:** 401–423.

Bouchez, J., V. Galy, R. G. Hilton, J. Gaillardet, P. Moreira-Turcq, M. A. Pérez, C. France-Lanord, and L. Maurice. 2014. Source, transport and fluxes of Amazon River particulate organic carbon: Insights from river sediment depth-profiles. Geochim. Cosmochim. Acta **133:** 280–298.

Chikaraishi, Y., and H. Naraoka. 2006. Carbon and hydrogen isotope variation of plant biomarkers in a plant–soil system. Chem. Geol. **231:** 190–202.

Cole, J. J. and others 2007. Plumbing the global carbon cycle: Integrating inland waters into the terrestrial carbon budget. Ecosystems **10:** 172–185.

Collister, J. W., R. E. Summons, E. Lichtfouse, and J. M. Hayes. 1992. An isotopic biogeochemical study of the Green River oil shale. Org. Geochem. **19:** 265–276.

Collister, J. W., E. Lichtfouse, G. Hieshima, and J. M. Hayes. 1994a. Partial resolution of sources of *n*-alkanes in the saline portion of the Parachute Creek Member, Green River Formation (Piceance Creek Basin, Colorado). Org. Geochem. **21:** 645–659.

Collister, J. W., G. Rieley, B. Stern, G. Eglinton, and B. Fry. 1994b. Compound-specific $\delta^{13}C$ analyses of leaf lipids from plants with differing carbon dioxide metabolisms. Org. Geochem. **21:** 619–627.

870 Drenzek, N. J., D. B. Montluçon, M. B. Yunker, R. W. Macdonald, and T. I. Eglinton. 2007.
871 Constraints on the origin of sedimentary organic carbon in the Beaufort Sea from
872 coupled molecular ^{13}C and ^{14}C measurements. Mar. Chem. **103:** 146–162.
873 Drenzek, N. J., K. A. Hughen, D. B. Montluçon, J. R. Southon, G. M. dos Santos, E. R. M.
874 Druffel, L. Giosan, and T. I. Eglinton. 2009. A new look at old carbon in active margin
875 sediments. Geology **37:** 239–242.
876 Eglinton, G., and R. J. Hamilton. 1967. Leaf epicuticular waxes. Science **156:** 1322−1335.
877 Feng, X., B. C. Benitez-Nelson, D. B. Montluçon, F. G. Prahl, A. P. McNichol, L. Xu, D. J.
878 Repeta, and T. I. Eglinton. 2013a. ^{14}C and ^{13}C characteristics of higher plant biomarkers
879 in Washington margin surface sediments. Geochim. Cosmochim. Acta **105:** 14–30.
880 Feng, X. and others 2013b. Differential mobilization of terrestrial carbon pools in Eurasian
881 Arctic river basins. Proc. Natl. Acad. Sci. **110:** 14168−14173.
882 Freeman, K. H., and L. A. Colarusso. 2001. Molecular and isotopic records of C_4 grassland
883 expansion in the late miocene. Geochim. Cosmochim. Acta **65:** 1439–1454.
884 Galy, V., T. Eglinton, C. France-Lanord, and S. Sylva. 2011. The provenance of vegetation
885 and environmental signatures encoded in vascular plant biomarkers carried by the
886 Ganges–Brahmaputra rivers. Earth Planet. Sci. Lett. **304:** 1–12.
887 Galy, V., and T. I. Eglinton. 2011. Protracted storage of biospheric carbon in the
888 Ganges-Brahmaputra basin. Nat. Geosci. **4:** 843–847.
889 Galy, V., B. Peucker-Ehrenbrink, and T. I. Eglinton. 2015. Global carbon export from the
890 terrestrial biosphere controlled by erosion. Nature **521:** 204–207.

Gelpi, E., H. Schneider, J. Mann, and J. Oro. 1970. Hydrocarbons of geochemical significance in microscopic algae. Phytochemistry **9:** 603–612.

Goñi, M. A., and S. Montgomery. 2000. Alkaline CuO oxidation with a microwave digestion system: lignin analyses of geochemical samples. Anal. Chem. **72:** 3116-3121.

Gong, M., L. Zhang, and P. Gong. 2006. Sources and spatial trends of *n*-alkanes in suspended particulate matter in the Huanghe River. Periodical of Ocean University of China **36:** 139–142 (in Chinese with English abstract).

Gustafsson, Ö., B. E. van Dongen, J. E. Vonk, O. V. Dudarev, and I. P. Semiletov. 2011. Widespread release of old carbon across the Siberian Arctic echoed by its large rivers. Biogeosciences **8:** 1737–1743.

Hossler, K., and J. E. Bauer. 2012. Estimation of riverine carbon and organic matter source contributions using time-based isotope mixing models. Journal of Geophysical Research: Biogeosciences **117:** G03035.

Hotchkiss, E. R., R. O. Hall Jr, R. A. Sponseller, D. Butman, J. Klaminder, H. Laudon, M. Rosvall, and J. Karlsson. 2015. Sources of and processes controlling CO_2 emissions change with the size of streams and rivers. Nat. Geosci. **8:** 696–699.

Hou, J., Y. Huang, C. Brodsky, M. R. Alexandre, A. P. McNichol, J. W. King, F. S. Hu, and J. Shen. 2010. Radiocarbon dating of individual lignin phenols: A new approach for establishing chronology of late quaternary lake sediments. Anal. Chem. **82:** 7119–7126.

Hu, B., G. Li, J. Li, J. Bi, J. Zhao, and R. Bu. 2012a. Provenance and climate change inferred from Sr–Nd–Pb isotopes of late Quaternary sediments in the Huanghe (Yellow River) Delta, China. Quat. Res. **78:** 561–571.

913 Hu, L., X. Shi, Z. Yu, T. Lin, H. Wang, D. Ma, Z. Guo, and Z. Yang. 2012b. Distribution of
914 sedimentary organic matter in estuarine–inner shelf regions of the East China Sea:
915 Implications for hydrodynamic forces and anthropogenic impact. Mar. Chem. **142–144:**
916 29–40.
917 Jia, W., and P. Peng. 2005. Molecular structure of kerogens from source rocks of the Tarim
918 Basin: A study by Py-GC-MS and methylation-Py-GC-MS. Sci. China Ser. D-Earth Sci.
919 **48:** 313–325.
920 Kao, S. J., and K. K. Liu. 1996. Particulate organic carbon export from a subtropical
921 mountainous river (Lanyang Hsi) in Taiwan. Limnol. Oceanogr. **41:** 1749–1757.
922 Keil, R. G., L. M. Mayer, P. D. Quay, J. E. Richey, and J. I. Hedges. 1997. Loss of organic
923 matter from riverine particles in deltas. Geochim. Cosmochim. Acta **61:** 1507–1511.
924 Komada, T., M. R. Anderson, and C. L. Dorfmeier. 2008. Carbonate removal from coastal
925 sediments for the determination of organic carbon and its isotopic signatures, $\delta^{13}C$ and
926 $\Delta^{14}C$: comparison of fumigation and direct acidification by hydrochloric acid. Limnol.
927 Oceanogr. **6:** 254–262.
928 Kusch, S., J. Rethemeyer, E. Schefuß, and G. Mollenhauer. 2010. Controls on the age of
929 vascular plant biomarkers in Black Sea sediments. Geochim. Cosmochim. Acta **74:**
930 7031–7047.
931 Lamoureux, S. F., and M. J. Lafrenière. 2014. Seasonal fluxes and age of particulate organic
932 carbon exported from Arctic catchments impacted by localized permafrost slope
933 disturbances. Environ. Res. Lett. **9:** 045002.

Liu, W., Z. An, W. Zhou, M. J. Head, and D. Cai. 2003. Carbon isotope and C/N ratios of suspended matter in rivers: an indicator of seasonal change in C_4/C_3 vegetation. Appl. Geochem. **18:** 1241–1249.

Liu, W., Y. Ning, Z. An, Z. Wu, H. Lu, and Y. Cao. 2005. Carbon isotopic composition of modern soil and paleosol as a response to vegetation change on the Chinese Loess Plateau. Sci. China Ser. D-Earth Sci. **48:** 93–99.

Liu, W., H. Yang, Y. Ning, and Z. An. 2007. Contribution of inherent organic carbon to the bulk $\delta^{13}C$ signal in loess deposits from the arid western Chinese Loess Plateau. Org. Geochem. **38:** 1571–1579.

Ludwig, W., J.-L. Probst, and S. Kempe. 1996. Predicting the oceanic input of organic carbon by continental erosion. Glob. Biogeochem. Cycles **10:** 23–41.

Martin, E. E., A. E. Ingalls, J. E. Richey, R. G. Keil, G. M. Santos, L. T. Truxal, S. R. Alin, and E. R. Druffel. 2013. Age of riverine carbon suggests rapid export of terrestrial primary production in tropics. Geophys. Res. Lett. **40:** 5687–5691.

Mayorga, E., A. K. Aufdenkampe, C. A. Masiello, A. V. Krusche, J. I. Hedges, P. D. Quay, J. E. Richey, and T. A. Brown. 2005. Young organic matter as a source of carbon dioxide outgassing from Amazonian rivers. Nature **436:** 538–541.

Milliman, J. D., Q. Yun-Shan, R. Mei-E, and Y. Saito. 1987. Man's Influence on the Erosion and Transport of Sediment by Asian Rivers: The Yellow River (Huanghe) Example. The Journal of Geology **95:** 751–762.

Moreira-Turcq, P., M. P. Bonnet, M. Amorim, M. Bernardes, C. Lagane, L. Maurice, M. Perez, and P. Seyler. 2013. Seasonal variability in concentration, composition, age, and

fluxes of particulate organic carbon exchanged between the floodplain and Amazon River. Glob. Biogeochem. Cycles **27:** 119–130.

Moyer, R. P., J. E. Bauer, and A. G. Grottoli. 2013. Carbon isotope biogeochemistry of tropical small mountainous river, estuarine, and coastal systems of Puerto Rico. Biogeochemistry **112:** 589–612.

Otto, A., and M. Simpson. 2005. Degradation and preservation of vascular plant-derived biomarkers in grassland and forest soils from western Canada. Biogeochemistry **74:** 377–409.

Pearson, A., and T. I. Eglinton. 2000. The origin of *n*-alkanes in Santa Monica Basin surface sediment: a model based on compound-specific $\Delta^{14}C$ and $\delta^{13}C$ data. Org. Geochem. **31:** 1103–1116.

Peng, J., S. Chen, and P. Dong. 2010. Temporal variation of sediment load in the Yellow River basin, China, and its impacts on the lower reaches and the river delta. CATENA **83:** 135–147.

Ran, L., X. X. Lu, H. Sun, J. Han, R. Li, and J. Zhang. 2013. Spatial and seasonal variability of organic carbon transport in the Yellow River, China. J. Hydrol. **498:** 76–88.

Raymond, P. A., and J. E. Bauer. 2001. Use of ^{14}C and ^{13}C natural abundances for evaluating riverine, estuarine, and coastal DOC and POC sources and cycling: a review and synthesis. Org. Geochem. **32:** 469–485.

Raymond, P. A., J. E. Bauer, N. F. Caraco, J. J. Cole, B. Longworth, and S. T. Petsch. 2004. Controls on the variability of organic matter and dissolved inorganic carbon ages in northeast US rivers. Mar. Chem. **92:** 353–366.

978 Ruff, M., S. Szidat, H. W. Gäggeler, M. Suter, H. A. Synal, and L. Wacker. 2010. Gaseous
979 radiocarbon measurements of small samples. Nucl. Instrum. Methods Phys. Res. **268:**
980 790–794.
981 Sanderman, J., K. A. Lohse, J. A. Baldock, and R. Amundson. 2009. Linking soils and
982 streams: Sources and chemistry of dissolved organic matter in a small coastal watershed.
983 Water Resour. Res. **45:** 450-455.
984 Schouten, S., W. C. M. Klein Breteler, P. Blokker, N. Schogt, W. I. C. Rijpstra, K. Grice, M.
985 Baas, and J. S. Sinninghe Damsté. 1998. Biosynthetic effects on the stable carbon
986 isotopic compositions of algal lipids: Implications for deciphering the carbon isotopic
987 biomarker record. Geochim. Cosmochim. Acta **62:** 1397–1406.
988 Shen, C., P. Ding, N. Wang, J. Han, S. Zhang, K. Liu, X. Ding, and D. Fu. 2007. Distribution
989 of comogenic ^{14}C and ^{10}Be of falling dust in beijing on april 16-17, 2006. Quat. Sci. **6:**
990 919–921.
991 Tao, S., T. I. Eglinton, D. B. Montluçon, C. McIntyre, and M. Zhao. 2015. Pre-aged soil
992 organic carbon as a major component of the Yellow River suspended load: Regional
993 significance and global relevance. Earth Planet. Sci. Lett. **414:** 77–86.
994 Tao, S., T. I. Eglinton, D. B. Montluçon, C. McIntyre, and M. Zhao. 2016. Diverse origins
995 and pre-depositional histories of organic matter in contemporary Chinese marginal sea
996 sediments. Geochim. Cosmochim. Acta **191:** 70–88.
997 Tarnocai, C., J. G. Canadell, E. A. G. Schuur, P. Kuhry, G. Mazhitova, and S. Zimov. 2009.
998 Soil organic carbon pools in the northern circumpolar permafrost region. Glob.
999 Biogeochem. Cycles **23:** GB2023.

Deleted: Nuclear Instruments & Methods in Physics Research

1002 Volkman, J. K., A. T. Revill, D. G. Holdsworth, and D. Fredericks. 2008. Organic matter
1003 sources in an enclosed coastal inlet assessed using lipid biomarkers and stable isotopes.
1004 Org. Geochem. **39:** 689–710.
1005 Vonk, J. E. and others 2014. Preferential burial of permafrost- derived organic carbon in
1006 Siberian- Arctic shelf waters. J. Geophys. Res. **119:** 8410–8421.
1007 Voss, B. M. and others 2015. Seasonal hydrology drives rapid shifts in the flux and
1008 composition of dissolved and particulate organic carbon and major and trace ions in the
1009 Fraser River, Canada. Biogeosciences **12:** 5597–5618.
1010 Wacker, L. and others 2010. MICADAS: Routine and high-precision radiocarbon dating.
1011 Radiocarbon **52:** 252–262.
1012 Wang, C. L., J. Tang, H. Wang, X. Yu, and S. Mi. 2010. Analysis of the seasonal variation of
1013 the Yellow River flux and the chlorophyll concentration in Laizhou Bay in 2007, p.
1014 243–251. IITA Second International Conference on Geoscience & Remote Sensing.
1015 Wang, H., Z. Yang, Y. Saito, J. P. Liu, and X. Sun. 2006. Interannual and seasonal variation
1016 of the Huanghe (Yellow River) water discharge over the past 50 years: Connections to
1017 impacts from ENSO events and dams. Glob. Planet. Change **50:** 212–225.
1018 Wang, H., Y. Saito, Y. Zhang, N. Bi, X. Sun, and Z. Yang. 2011. Recent changes of sediment
1019 flux to the western Pacific Ocean from major rivers in East and Southeast Asia. Earth Sci.
1020 Rev. **108:** 80–100.
1021 Wang, X., H. Ma, R. Li, Z. Song, and J. Wu. 2012. Seasonal fluxes and source variation of
1022 organic carbon transported by two major Chinese Rivers: The Yellow River and
1023 Changjiang (Yangtze) River. Glob. Biogeochem. Cycles **26:** GB2025.

1024 Wang, X., C. Luo, T. Ge, C. Xu, and Y. Xue. 2016. Controls on the sources and cycling of
1025 dissolved inorganic carbon in the Changjiang and Huanghe River estuaries, China: 14C
1026 and 13C studies. Limnol. Oceanogr. **61:** 1358–1374.
1027 Ward, N. D. and others 2013. Degradation of terrestrially derived macromolecules in the
1028 Amazon River. Nat. Geosci. **6:** 530–533.
1029 Wiesenberg, G. L. B., J. Schwarzbauer, M. W. I. Schmidt, and L. Schwark. 2004. Source and
1030 turnover of organic matter in agricultural soils derived from *n*-alkane/*n*-carboxylic acid
1031 compositions and C-isotope signatures. Org. Geochem. **35:** 1371–1393.
1032 Wu, L., Y. Huh, J. Qin, G. Du, and S. van Der Lee. 2005. Chemical weathering in the Upper
1033 Huang He (Yellow River) draining the eastern Qinghai-Tibet Plateau. Geochim.
1034 Cosmochim. Acta **69:** 5279–5294.
1035 Xu, J., J. Yang, and Y. Yan. 2006. Erosion and sediment yields as influenced by coupled
1036 eolian and fluvial processes: The Yellow River, China. Geomorphology **73:** 1–15.
1037 Zhang, J., W. W. Huang, R. Létolle, and C. Jusserand. 1995. Major element chemistry of the
1038 Huanghe (Yellow River), China–weathering processes and chemical fluxes. J. Hydrol.
1039 **168:** 173–203.
1040 Zhang, L., L. Wang, W.-J. Cai, D. Liu, and Z. Yu. 2013. Impact of human activities on
1041 organic carbon transport in the Yellow River. Biogeosciences **10:** 2513–2524.
1042 Zhang, X., H. Wang, H. Ru, and W. Zhao. 2010. Riparian C_4 Plants on the Mainstream of the
1043 Yellow River: Assemblage Characteristics and Their Indication on the Effects of
1044 Reservoirs. Journal of Wuhan Botanical Research **28:** 568–576 (in Chinese with English
1045 abstract).

Zhao, M., J. L. Mercer, G. Eglinton, M. J. Higginson, and C. Huang. 2006. Comparative molecular biomarker assessment of phytoplankton paleoproductivity for the last 160 kyr off Cap Blanc, NW Africa. Org. Geochem. **37:** 72–97.

Zou, L., M.-Y. Sun, and L. Guo. 2006. Temporal variations of organic carbon inputs into the upper Yukon River: Evidence from fatty acids and their stable carbon isotopic compositions in dissolved, colloidal and particulate phases. Org. Geochem. **37:** 944–956.

Acknowledgements

We would like to thank Dr. Zineng Yuan for sampling help; all members of Ion Beam Physics Laboratory at ETH for AMS measurements; Dr. Rui Bao for assistance with SA measurements, and Stewart Bishop and Madalina Jaggi for stable carbon isotope measurements. This work was supported by the National Key Research and Development Program of China (grant NO. 2016YFA0601403), by the National Natural Science Foundation of China (Grant No. 41506089, 41520104009, 41521064), the "111" Project (No. B13030), the Project Sponsored by the Scientific Research Foundation of Third Institute of Oceanography, SOA of China (NO. 2017013), and the Swiss National Science Foundation (SNF Grant No. 200021_140850). This is MCTL contribution #129.

Figure Captions

Fig. 1. The Yellow River basin and location of the Kenli sampling station (37.68°N, 118.52°E). The up-left panel is a map of the East Asia showing the Yellow River drainage

basin, coal-bearing areas within the watershed, and Chinese marginal seas.

Fig. 2. Temporal variations in water discharge and TSS at the middlestream Tongguan (the boundary of the middle-lower Yellow River, blue) and downstream Lijin station (red) during 2011 to 2013: (a) daily water discharge; (b) daily TSS; (c) monthly averaged discharge and (d) monthly averaged TSS. Our study period begins from June 2011 to July 2013, and includes three water and sediment regulation (WSR) periods (grey vertical bars) and two autumn natural high flow (NHF) periods (blue vertical bars). All data are provided by the YRCC (http://www.yellowriver.gov.cn/nishagonggao/). Monthly average water discharge was calculated based on the daily measurements, whereas monthly average TSS was calculated based on monthly sediment load (kg) divided by monthly discharge (Q; m^3).

Fig. 3. (a) Temporal variations of in situ discharge, in situ TSS and concentrations of various OC components. (b) Temporal variations of in situ discharge, in situ TSS and TOC normalized contents of various OC components. The solid line represents the first year of our study and dash line represents the second year of our study. The in situ TSS concentration and discharge were measured instantaneously, the in situ discharge was the daily value in specific sampling time collected from YRCC website; TSS was determined based on the weight of SPM on the filters and the volume of water filtered in specific sampling time.

Fig. 4. Temporal variations in $\delta^{13}C$ values of various biomarker compounds (*n*-FAs and *n*-alkanes) compared with that of POC from the Yellow River: (a) short-chain lipid

biomarkers; (b) long-chain lipid biomarkers. The solid line represents the first year of our study and dash line represents the second year of our study. Note: there is a break and a change of y-axis of Figure 4a.

Fig. 5. Temporal variation in radiocarbon contents (expressed as $\Delta^{14}C$ and conventional ^{14}C age) of various biomarker compounds compared with that of POC from the Yellow River. The solid line represents the first year of our study and dash line represents the second year of our study.

Fig. 6. Cross-plot of the stable isotopic compositions ($\delta^{13}C$) versus the radiocarbon compositions ($\Delta^{14}C$) of different organic components for POC from the Yellow River and for other putative source organic materials from northern China and from the Yellow River watershed. The latter includes published $\delta^{13}C$ compositions of typical C_3 and C_4 plants from the Chinese Loess Plateau (–27.1±2.4‰ for C_3 plants, n = 39; –12.7±2.1‰ for C_4 plants, n = 18; Liu et al. 2005), kerogen from the Tarim Basin with numerous petroleum source rocks in northwestern China (–28.0±1.6‰, n = 10; Jia and Peng, 2005), source rock from the mountains of the Qinghai plateau located in the upstream of the Yellow River (–21.2±1.2‰; Liu et al., 2007). For comparability in $\delta^{13}C$ between lipid biomarkers and bulk OM, a center value of 6‰ was added to $\delta^{13}C$ values of individual lipid compounds since ^{13}C isotopic fractionation effects ($\delta^{13}C_{bulk} - \delta^{13}C_{lipid}$) need to be taken in account. Modern plant sources are assigned a $\Delta^{14}C$ value of 0 ± 50‰, and ancient or fossil sources (ancient sedimentary rocks) have a $\Delta^{14}C$ value of -1000‰. Also shown are values for dust particles collected in Beijing (Shen et al. 2007).

Fig. 7. (a) Coupled isotope mass balance results for the temporal variations of the fractional contributions of contemporary biomass, pre-aged soil and fossil OC in the Yellow River suspended matter. Data points represent average values of all possible solution derived from three endmember mixing model calculation over a range of prescribed $\delta^{13}C_{Bulk} - \delta^{13}C_{lipid}$ offset (5–7‰). Warm and wet seasons correspond to summer June–August) and autumn (September–November), cold/dry seasons infer to winter (September–February) and spring (March−May). (b) Temporal variations of fluxes of contemporary biomass, pre-aged soil and fossil OC in the Yellow River suspended matter.

Fig. 8. Relationships between monthly discharges (Q) and monthly fluxes of different source OC (a) and TSS (b).

Fig. 9. Comparison of the time-series $\Delta^{14}C$ dataset of POC in different river systems in the world. All included data are only referred from temporal studies at fixed locations. *n* values indicate the number of time points: Yellow River (this study); Changjiang (Wang et al. 2012); Amazon (Mayorga et al. 2005; Moreira-Turcq et al. 2013); Mekong (Martin et al. 2013); Brahmaputra, Ganges and their tributaries such as Karnali, Kosi and Narayani (Ganges-Brahmaputra basin) (Galy and Eglinton 2011); Lanyang His (Kao and Liu 1996); Hudson, Parker and York Rivers (U.S.A.) (Raymond et al. 2004); Rio Loco and Rio Fajardo Rivers (Puerto Rico) (Moyer et al. 2013); East River, West River and their tributaries such as Ptamigan and Goose (Cape Bounty Arctic Watershed) (Lamoureux and Lafrenière 2014).

1137

Tables

Table 1. Sampling information and bulk organic carbon characteristics.

Month	Sampling date	Description	POC%	Surface area [m^2/g]	Monthly discharge [m^3/s]	Monthly TSS [g/L]
2011						
June*	2011/06/28	WSR	0.40	20.4	1820	10.26
September	2011/09/22	Flood event	0.33	17.3	1016	7.93
November	2011/11/17		0.45	27.4	998	1.96
2012						
January	2012/01/13		0.32	18.1	703	1.94
April	2012/04/22		0.47	28.8	288	1.76
June	2012/06/19		0.27	16.8	1324	6.96
June*	2012/06/27	WSR	0.32	18.4		
October	2012/10/13		0.30	24.3	898	4.15
2013						
January	2013/01/ 04		0.26	22.1	592	0.85
April	2013/04/28		0.37	25.9	261	1.55
June	2013/06/19		0.28	20.2	1623	7.74
July*	2013/07/04	WSR	0.31	24.8		

* WSR: water and sediment regulation period

Table 2. Results from the Monte Carlo source apportionment calculations (given as mean ± standard deviation) for the total contemporary biomass OC in two SPM exported by the Yellow River (October 2012 and April 2013). The end-members and the standard deviations used in the simulations are further explained and referred to in the main text.

Month	Season	Fractions		
		$F_{aquatic}$	f_{C3}	f_{C4}
October 2012	Autumn	0.29±0.03	0.31±0.10	0.40±0.10
April 2013	Spring	0.46±0.02	0.13±0.06	0.41±0.06

Table 3. Monthly TSS fluxes and estimated monthly fluxes of modern biomass OC, pre-aged soil OC and fossil OC carried by the Yellow River SPM.

Month	Monthly Q [10^8 m^3]	Monthly TSS [Mt]	Modern OC [10^4 t/yr]	Pre-aged OC [10^4 t/yr]	Fossil OC [10^4 t/yr]
June	17.06	17.50	1.19±0.73	3.32±2.27	2.44±1.47
July	28.12	26.50	0.83±1.22	2.32±3.81	1.45±2.47
August	12.35	1.57	0.11±0.56	0.29±1.76	0.19±1.14
September	27.73	22.00	0.81±1.2	2.24±3.75	1.41±2.43
October	32.14	12.00	1.14±1.44	3.21±4.50	2.00±2.91
November	24.60	4.82	0.61±1.05	1.66±3.27	1.05±2.12
December	27.86	7.42	0.82±1.21	2.26±3.77	1.42±2.45
January	19.34	3.75	0.34±0.82	0.89±2.55	0.58±1.66
February	7.31	0.66	0.03±0.43	0.15±1.33	0.08±0.87
March	9.24	1.31	0.05±0.47	0.17±1.48	0.11±0.96
April	7.78	1.37	0.03±0.44	0.15±1.36	0.08±0.89
May	14.60	3.16	0.16±0.64	0.43±1.99	0.29±1.29
2011.6~2012.5	**228.1**	**102.1**	**6.1±0.64（18%）**	**17.1±6.4（50%）**	**11.1±9.9（32%）**
June	34.21	23.80	1.31±1.56	3.74±4.87	2.31±3.16
July	53.57	56.50	3.58±2.99	10.62±9.33	6.43±6.02
August	47.94	65.90	2.80±2.52	8.25±7.86	5.02±5.07
September	30.33	10.60	0.99±1.34	2.79±4.18	1.74±2.71
October	22.47	9.32	0.49±0.95	1.32±2.96	0.84±1.92
November	14.59	2.62	0.16±0.64	0.43±1.99	0.28±1.29
December	20.89	4.04	0.41±0.88	1.09±2.75	0.70±1.79
January	15.13	1.29	0.18±0.66	0.47±2.05	0.31±1.33
February	14.90	2.34	0.17±0.65	0.46±2.02	0.30±1.32
March	10.10	1.56	0.06±0.50	0.20±1.55	0.12±1.01
April	7.05	1.09	0.03±0.42	0.15±1.31	0.08±0.85
May	8.76	1.42	0.04±0.46	0.16±1.44	0.10±0.94

June	36.55	28.30	1.53±1.71	4.38±5.32	2.70±3.45
2012.6~2013.5	**279.9**	**180.5**	**10.2±4.8（18%）**	**29.7±14.4（51%）**	**18.2±15.0（31%）**

1151

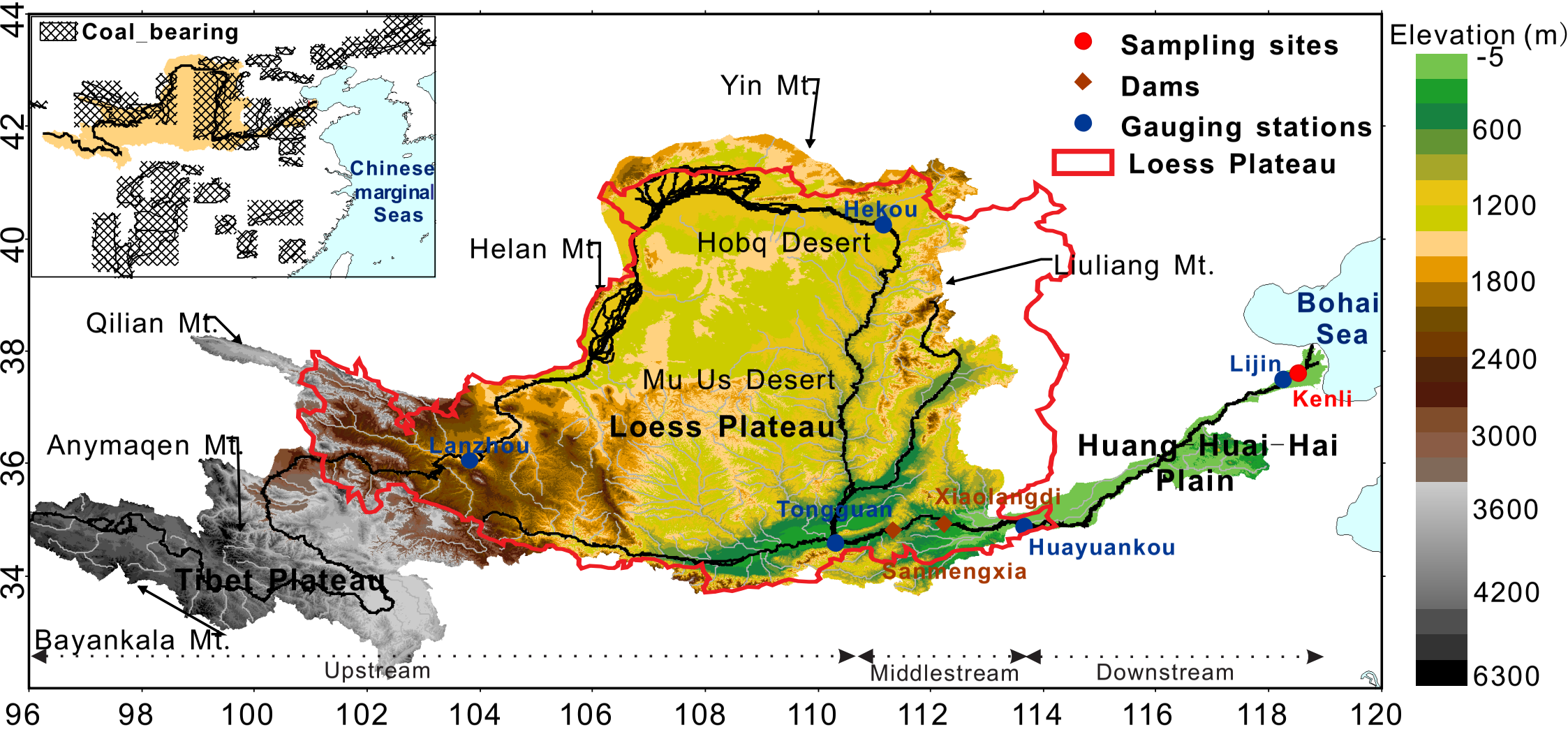
Coal_bearing
Chinese marginal Seas
Sampling sites
Dams
Gauging stations
Loess Plateau
Elevation (m)
-5
600
1200
1800
2400
3000
3600
4200
6300
Yin Mt.
Helan Mt.
Liuliang Mt.
Qilian Mt.
Anymaqen Mt.
Bayankala Mt.
Hobq Desert
Mu Us Desert
Loess Plateau
Tibet Plateau
Huang-Huai-Hai Plain
Bohai Sea
Hekou
Lanzhou
Tongguan
Xiaolangdi
Sanmengxia
Huayuankou
Lijin
Kenli
Upstream
Middlestream
Downstream
44
42
40
38
36
34
96
98
100
102
104
106
108
110
112
114
116
118
120

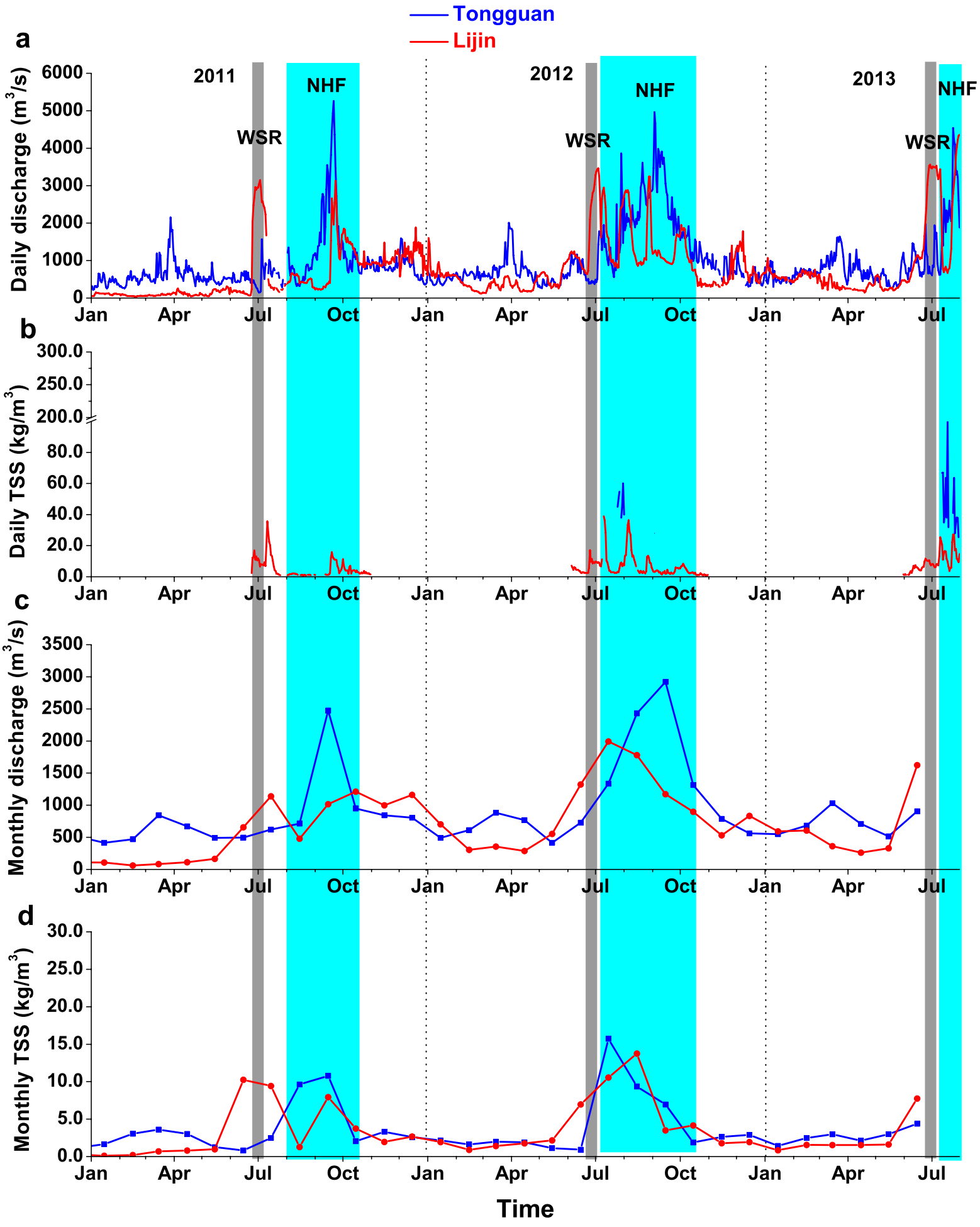
Tongguan
Lijin
a
Daily discharge (m3/s)
2011
2012
2013
NHF
WSR
b
Daily TSS (kg/m3)
c
Monthly discharge (m3/s)
d
Monthly TSS (kg/m3)
Jan
Apr
Jul
Oct
Time

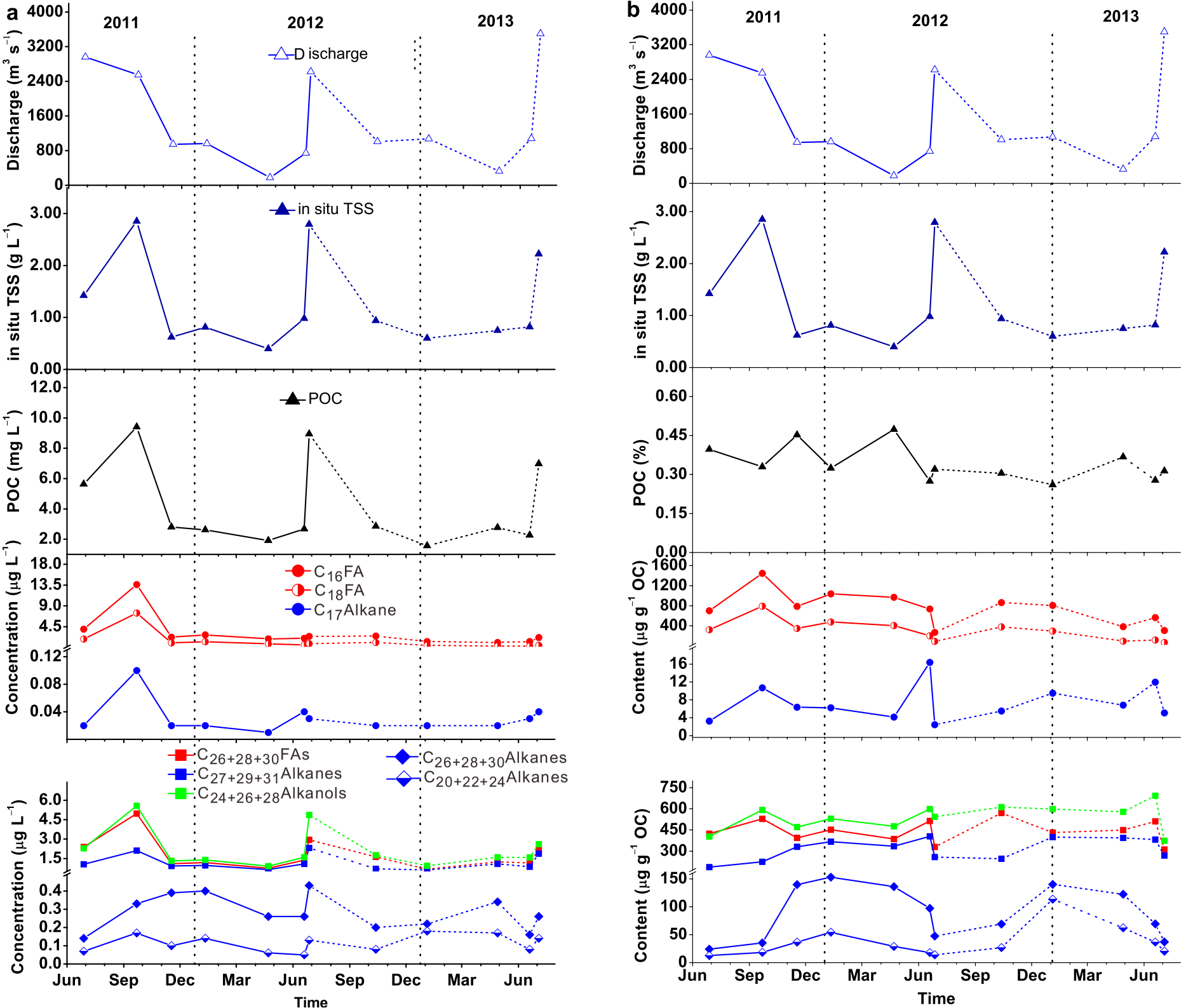
a
b
2011
2012
2013
Discharge ($m^3 s^{-1}$)
D ischarge
in situ TSS ($g L^{-1}$)
in situ TSS
POC ($mg L^{-1}$)
POC
POC (%)
Concentration ($\mu g L^{-1}$)
$C_{16}FA$
$C_{18}FA$
$C_{17}Alkane$
Content ($\mu g g^{-1}$ OC)
$C_{26+28+30}FAs$
$C_{27+29+31}Alkanes$
$C_{24+26+28}Alkanols$
$C_{26+28+30}Alkanes$
$C_{20+22+24}Alkanes$
Jun
Sep
Dec
Mar
Jun
Sep
Dec
Mar
Jun
Time

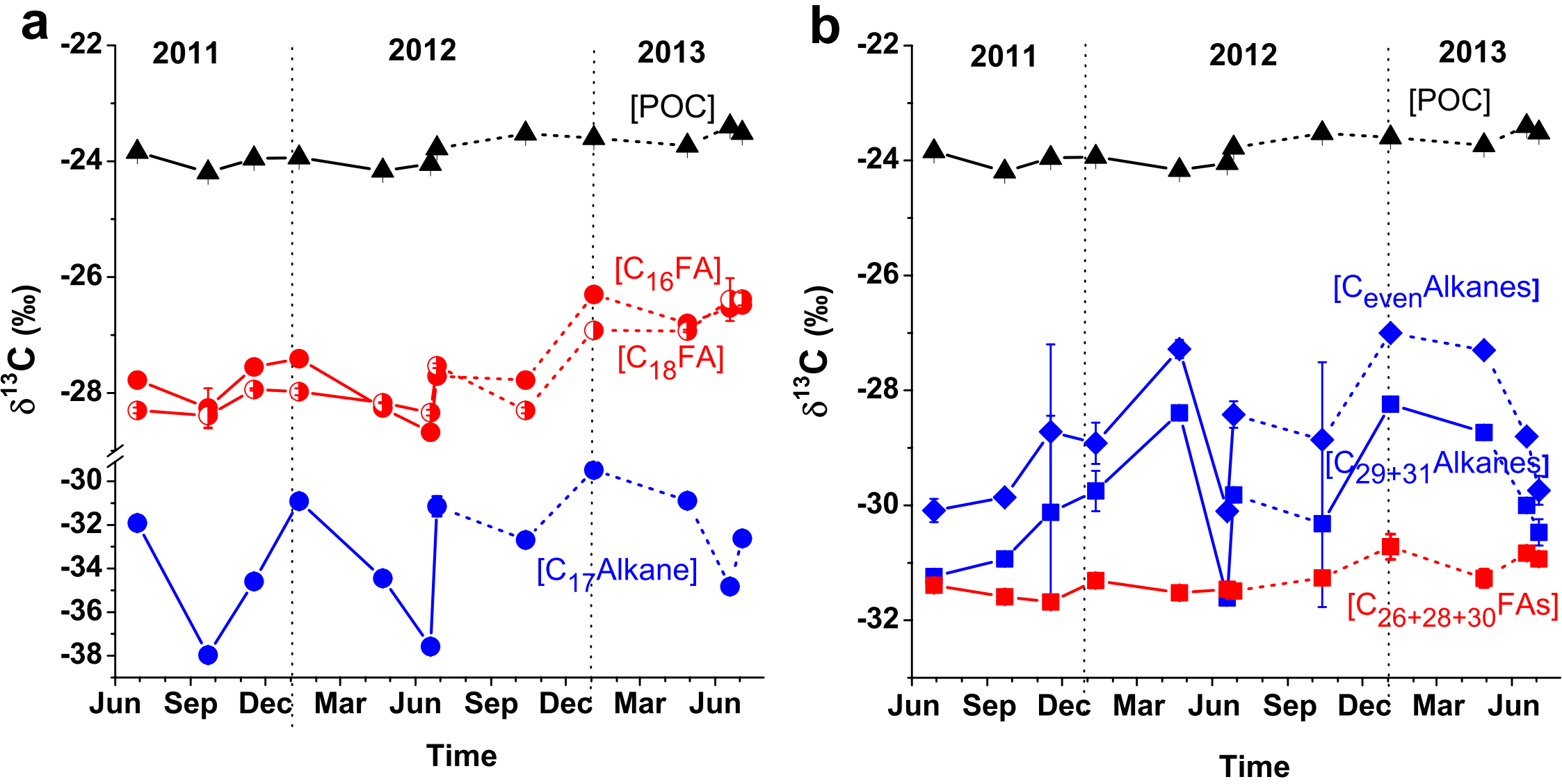
a
2011
2012
2013
[POC]
[C16FA]
[C18FA]
[C17Alkane]
δ13C (‰)
-22
-24
-26
-28
-30
-32
-34
-36
-38
Jun
Sep
Dec
Mar
Jun
Sep
Dec
Mar
Jun
Time
b
2011
2012
2013
[POC]
[Ceven Alkanes]
[C29+31 Alkanes]
[C26+28+30 FAs]
δ13C (‰)
-22
-24
-26
-28
-30
-32
Jun
Sep
Dec
Mar
Jun
Sep
Dec
Mar
Jun
Time

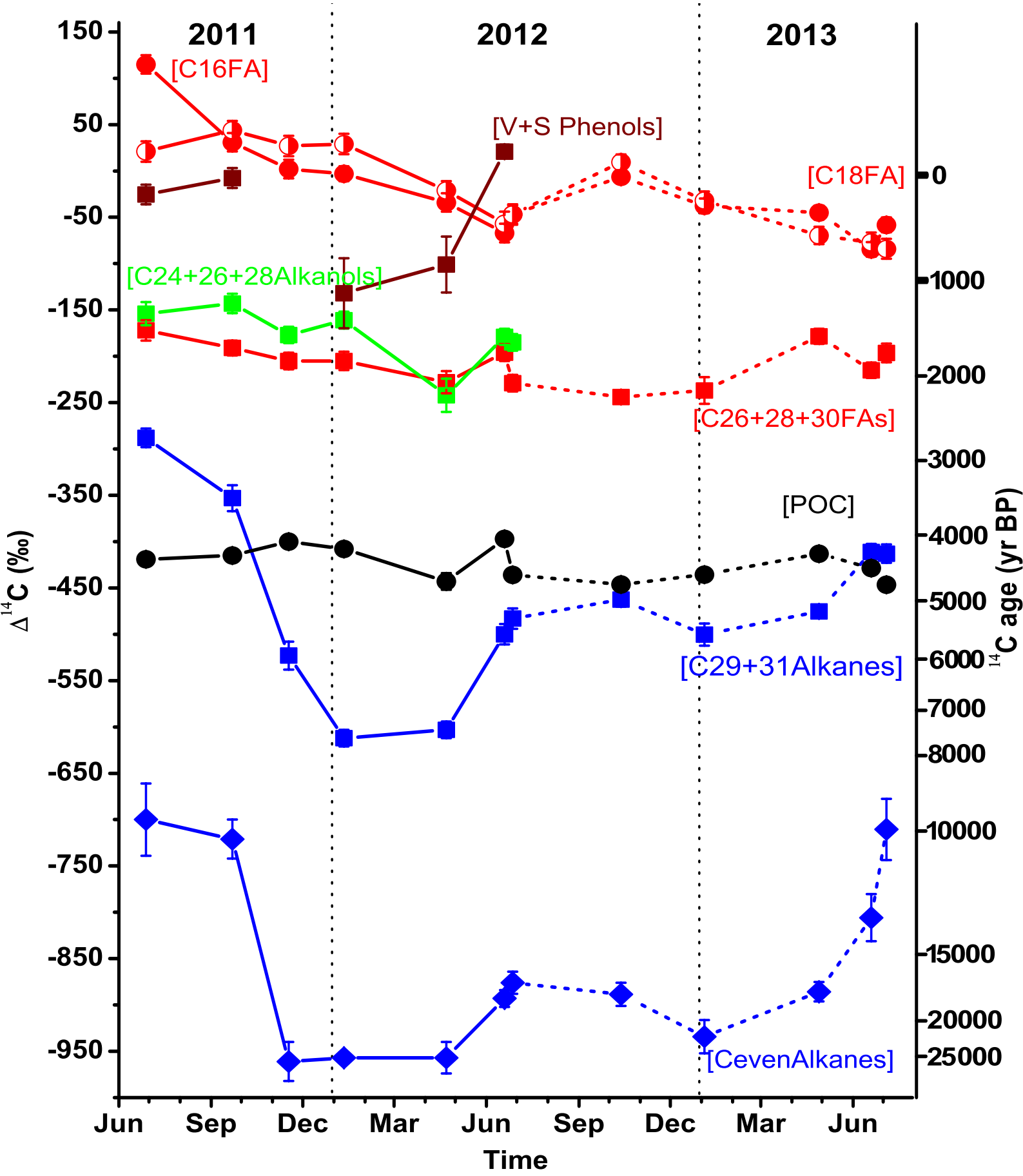
2011
2012
2013
[C16FA]
[V+S Phenols]
[C18FA]
[C24+26+28Alkanols]
[C26+28+30FAs]
[POC]
[C29+31Alkanes]
[CevenAlkanes]
150
50
-50
-150
-250
-350
-450
-550
-650
-750
-850
-950
0
1000
2000
3000
4000
5000
6000
7000
8000
10000
15000
20000
25000
Jun
Sep
Dec
Mar
Jun
Sep
Dec
Mar
Jun
Time
Δ14C (‰)
14C age (yr BP)

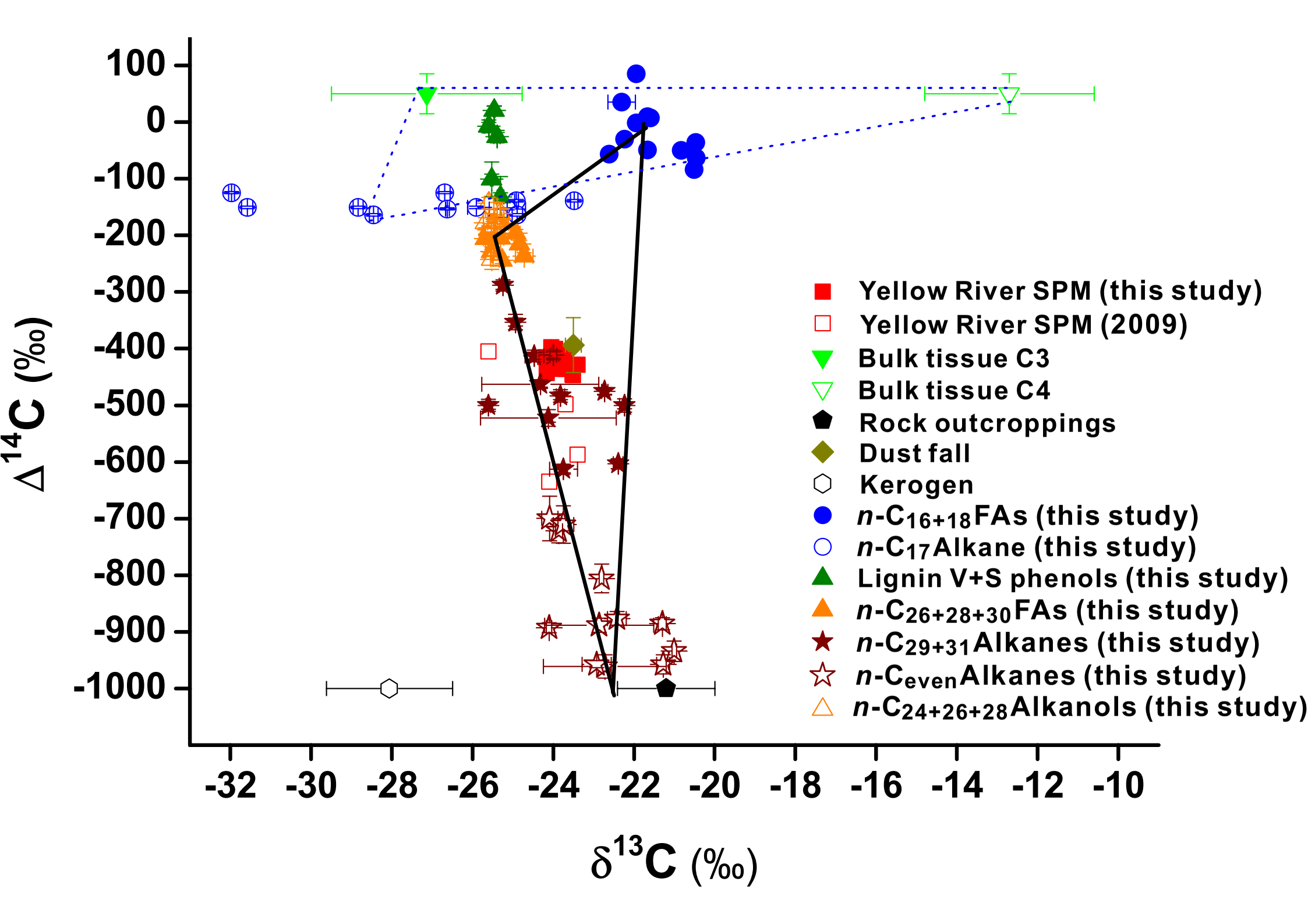
100
0
-100
-200
-300
-400
-500
-600
-700
-800
-900
-1000
Δ14C (‰)
-32
-30
-28
-26
-24
-22
-20
-18
-16
-14
-12
-10
δ13C (‰)
Yellow River SPM (this study)
Yellow River SPM (2009)
Bulk tissue C3
Bulk tissue C4
Rock outcroppings
Dust fall
Kerogen
n-C16+18FAs (this study)
n-C17Alkane (this study)
Lignin V+S phenols (this study)
n-C26+28+30FAs (this study)
n-C29+31Alkanes (this study)
n-Ceven Alkanes (this study)
n-C24+26+28Alkanols (this study)

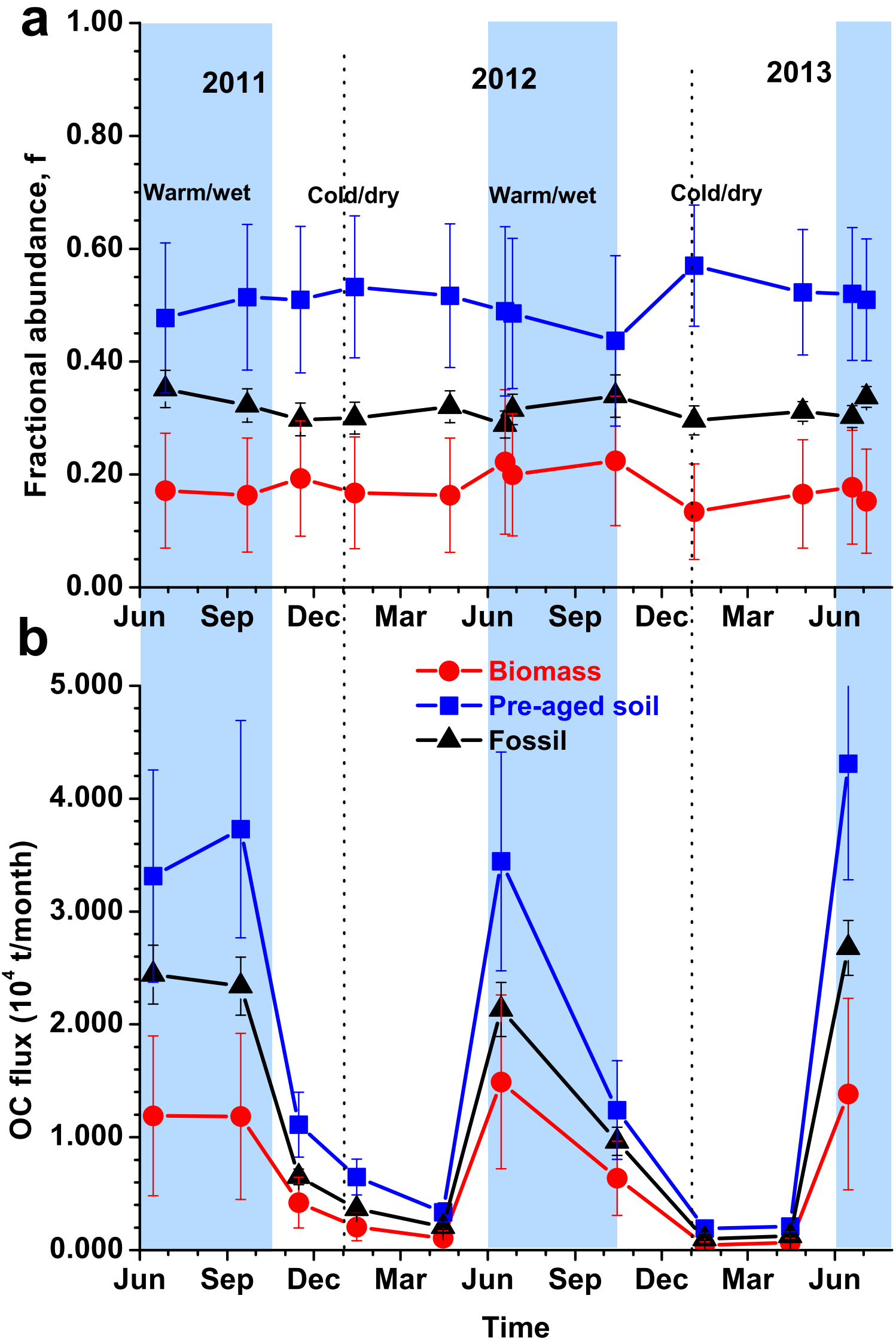
a
b
2011
2012
2013
Warm/wet
Cold/dry
Warm/wet
Cold/dry
Fractional abundance, f
1.00
0.80
0.60
0.40
0.20
0.00
Jun
Sep
Dec
Mar
Jun
Sep
Dec
Mar
Jun
Biomass
Pre-aged soil
Fossil
OC flux (10^4 t/month)
5.000
4.000
3.000
2.000
1.000
0.000
Time

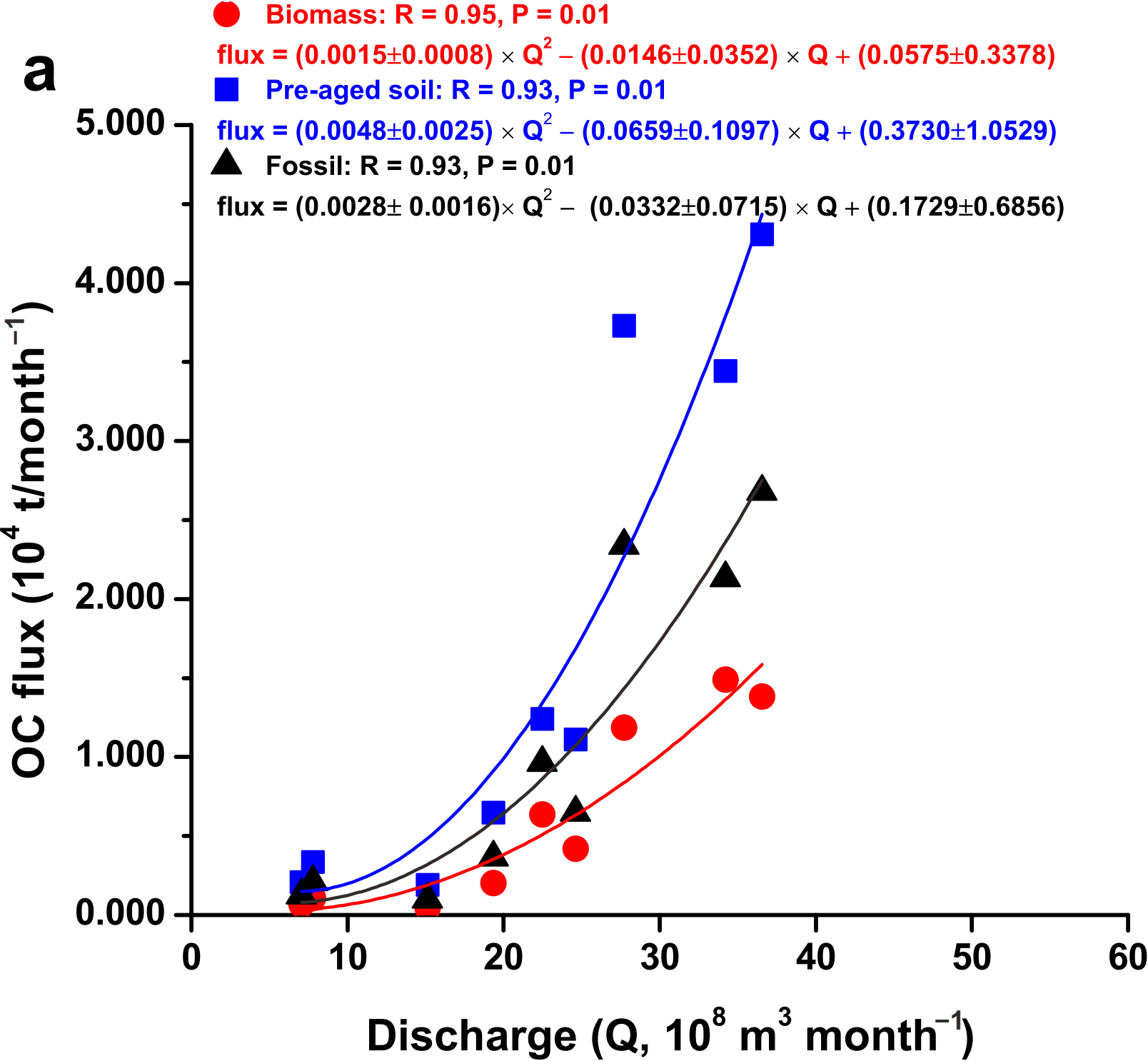
a
Biomass: R = 0.95, P = 0.01
flux = (0.0015±0.0008) × Q² – (0.0146±0.0352) × Q + (0.0575±0.3378)
Pre-aged soil: R = 0.93, P = 0.01
flux = (0.0048±0.0025) × Q² – (0.0659±0.1097) × Q + (0.3730±1.0529)
Fossil: R = 0.93, P = 0.01
flux = (0.0028± 0.0016)× Q² – (0.0332±0.0715) × Q + (0.1729±0.6856)
OC flux (10⁴ t/month⁻¹)
5.000
4.000
3.000
2.000
1.000
0.000
0
10
20
30
40
50
60
Discharge (Q, 10⁸ m³ month⁻¹)

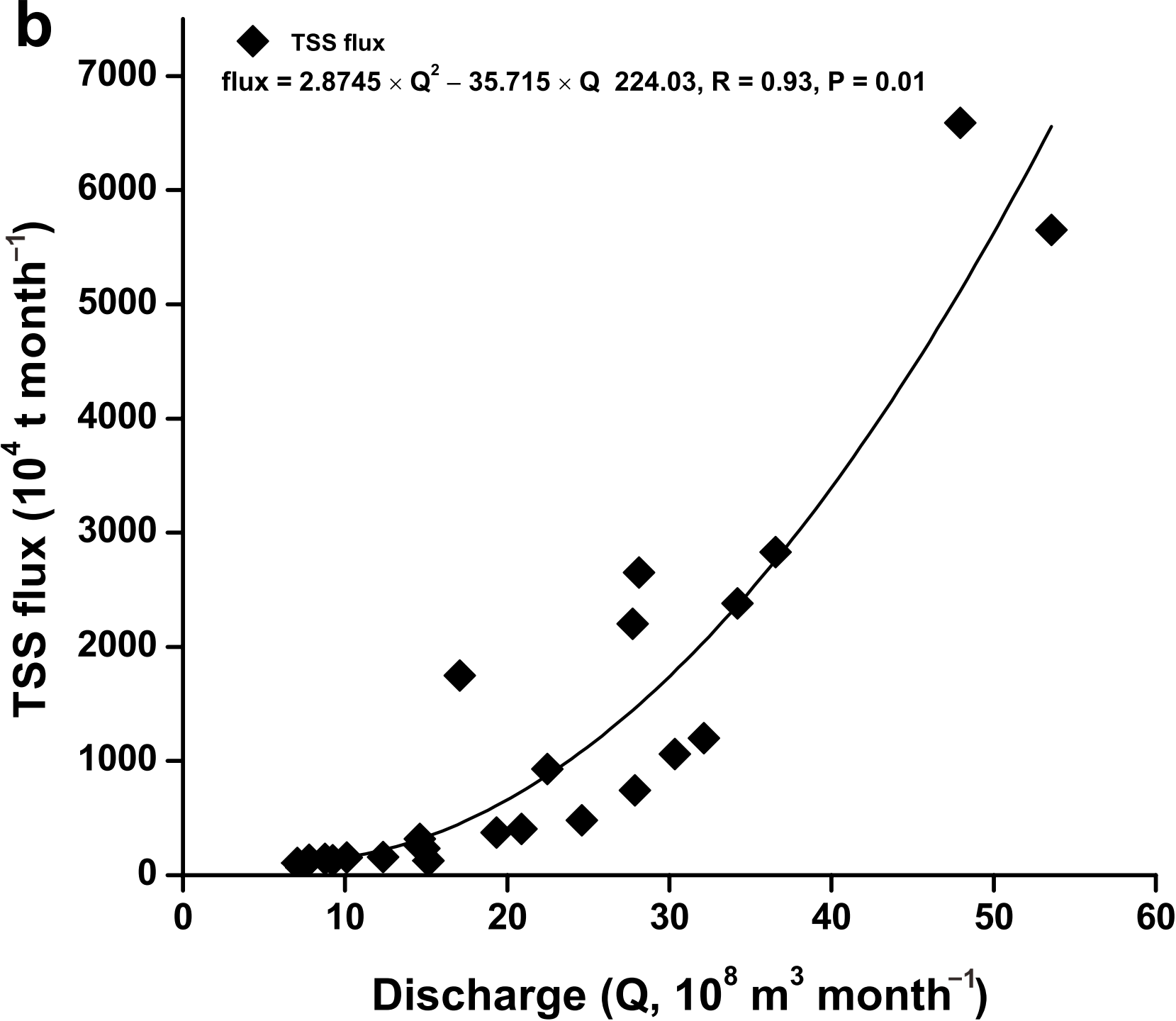
b
TSS flux
flux = 2.8745 × Q² – 35.715 × Q 224.03, R = 0.93, P = 0.01
TSS flux (10⁴ t month⁻¹)
Discharge (Q, 10⁸ m³ month⁻¹)
0
1000
2000
3000
4000
5000
6000
7000
0
10
20
30
40
50
60

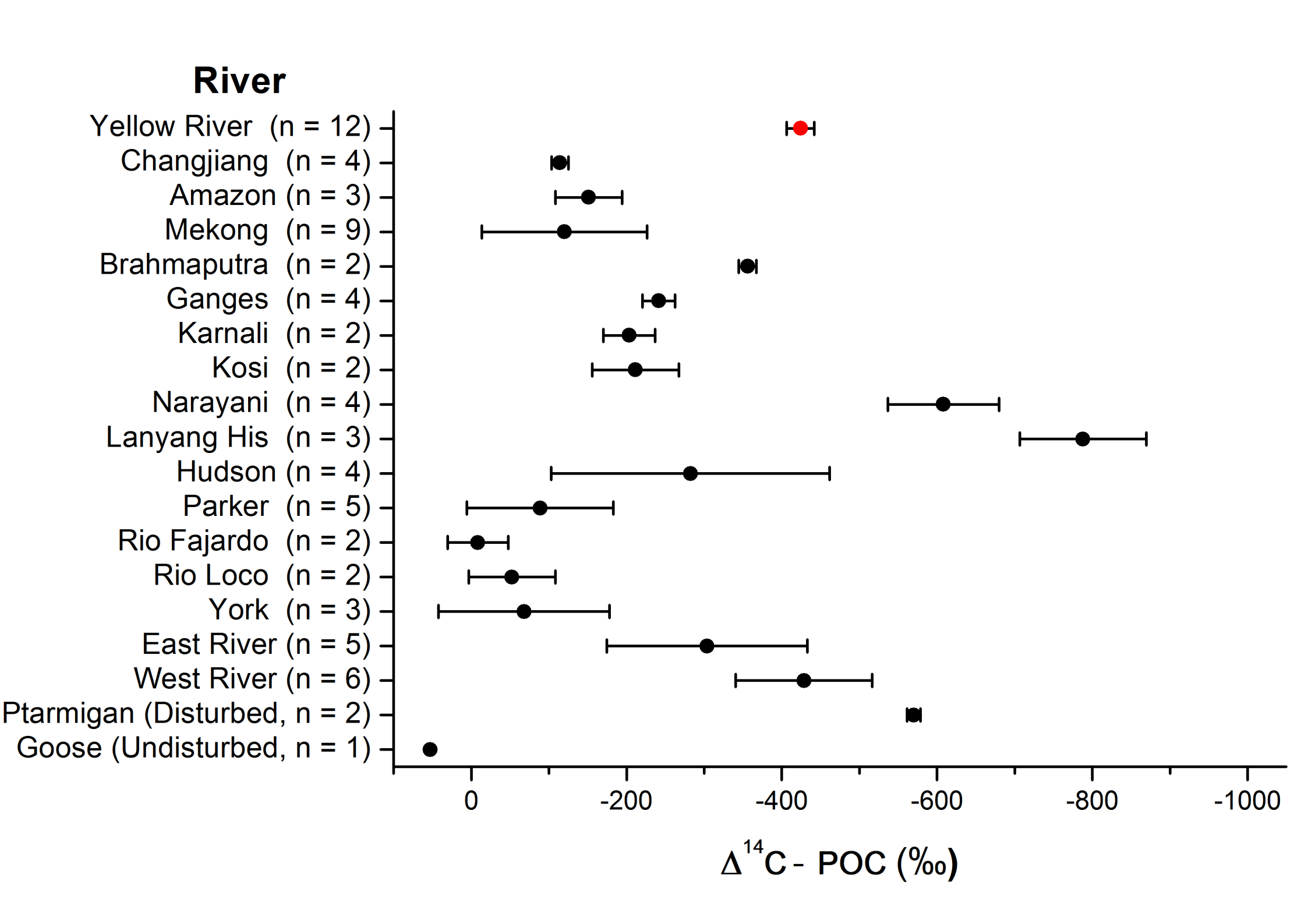
River
Yellow River (n = 12)
Changjiang (n = 4)
Amazon (n = 3)
Mekong (n = 9)
Brahmaputra (n = 2)
Ganges (n = 4)
Karnali (n = 2)
Kosi (n = 2)
Narayani (n = 4)
Lanyang His (n = 3)
Hudson (n = 4)
Parker (n = 5)
Rio Fajardo (n = 2)
Rio Loco (n = 2)
York (n = 3)
East River (n = 5)
West River (n = 6)
Ptarmigan (Disturbed, n = 2)
Goose (Undisturbed, n = 1)
0
-200
-400
-600
-800
-1000
Δ14C - POC (‰)

Supplementary information (SI)

Content (Caption):

The supplementary materials include four figures and one table:

Fig. S1. Hierarchical cluster analysis on TOC normalized contents of different lipid biomarkers.

Fig. S2. Hierarchical cluster analysis on stable carbon isotopes of different lipid biomarkers.

Fig. S3. Plots of typical biomarker stable carbon and radiocarbon isotopic compositions *v.s.* monthly discharge and monthly TSS.

Fig. S4. Examples of Monte Carlo probability density functions for the fractions f_B, f_S and f_F to the POC from the Yellow River at different times.

Table S1. Coupled isotope mass balance results from the Monte Carlo source apportionment calculations for the fractional contributions of three different OC components.

Figures

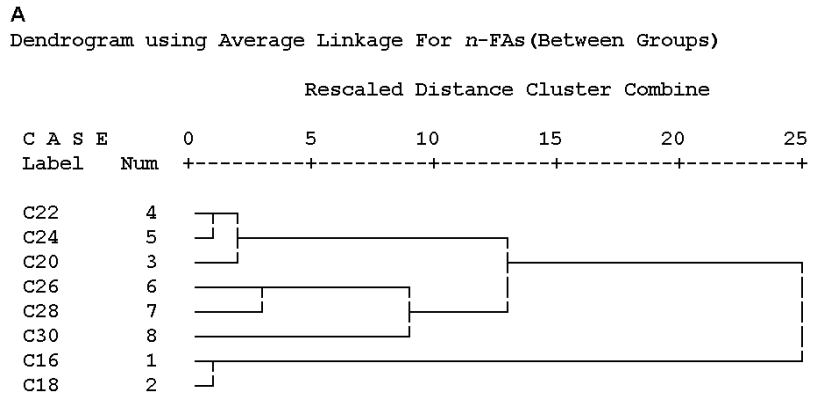

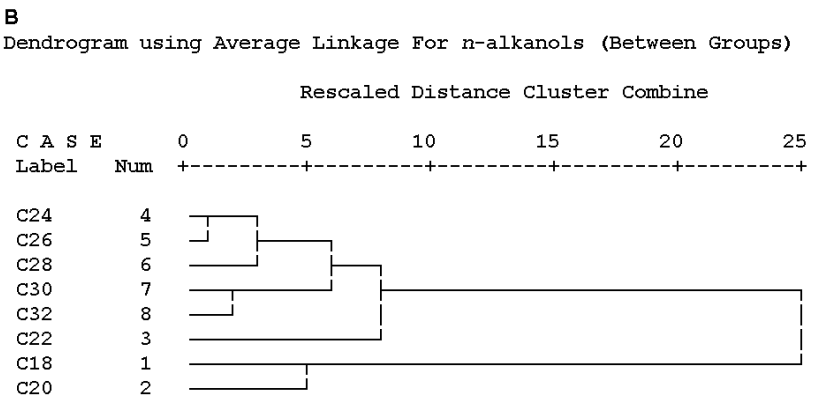

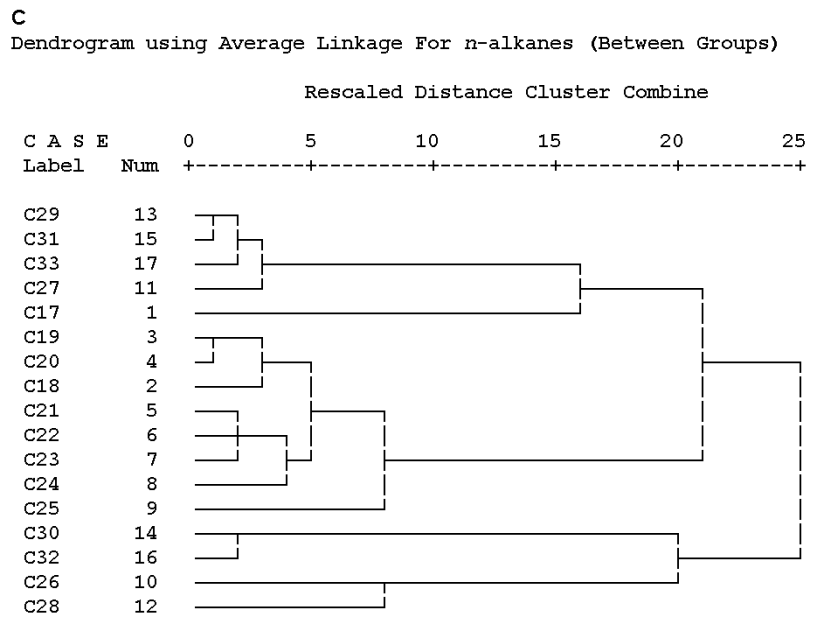

Fig. S1. Hierarchical cluster analysis on TOC normalized contents of different lipid biomarkers. (a) *n*-FAs, (b) *n*-alkanols and (c) *n*-alkanes.

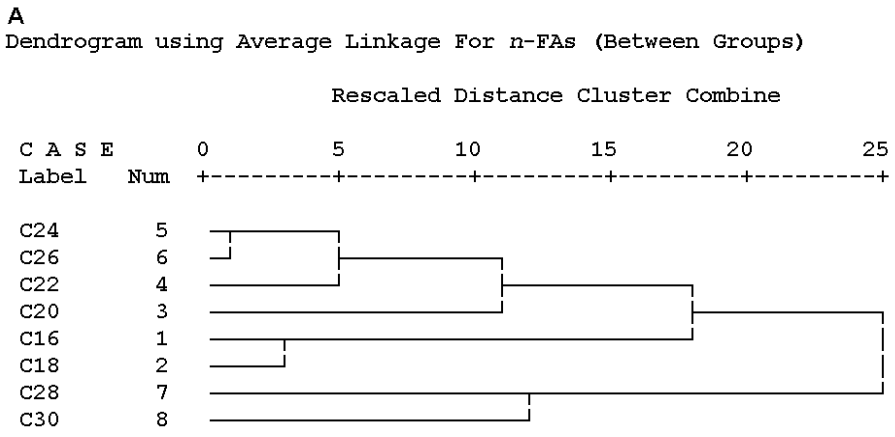

1

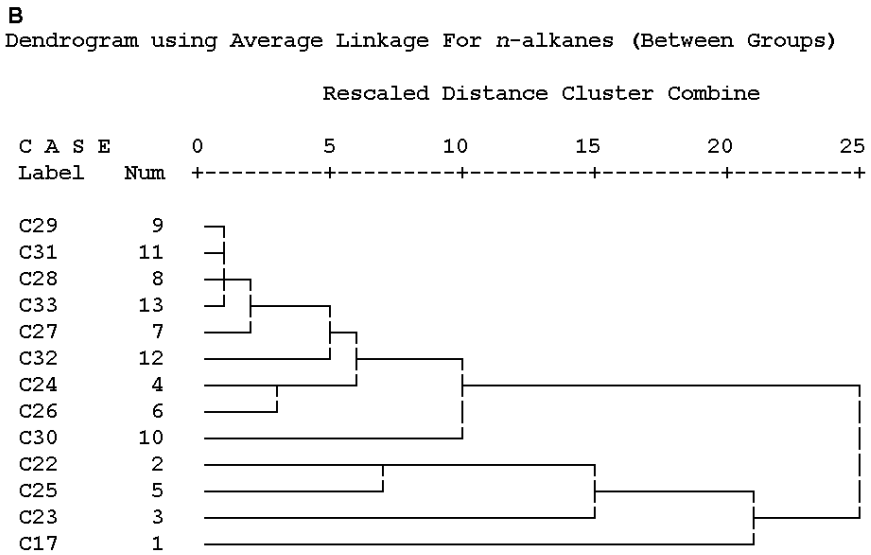

2

3 **Fig. S2.** Hierarchical cluster analysis on stable carbon isotopes of different lipid biomarkers. (a) *n*-FAs and (b)

4 *n*-alkanes.

5

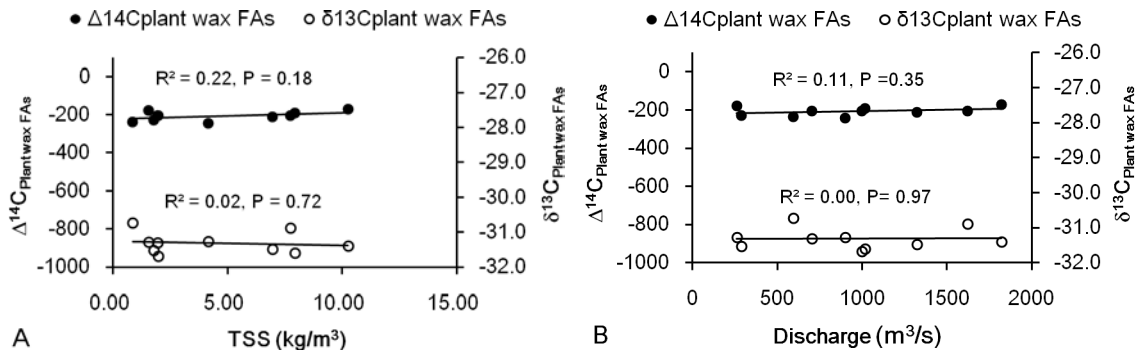
● Δ14Cplant wax FAs ○ δ13Cplant wax FAs
R² = 0.22, P = 0.18
R² = 0.02, P = 0.72
Δ14CPlant wax FAs
δ13CPlant wax FAs
TSS (kg/m3)
A
● Δ14Cplant wax FAs ○ δ13Cplant wax FAs
R² = 0.11, P =0.35
R² = 0.00, P= 0.97
Δ14CPlant wax FAs
δ13CPlant wax FAs
Discharge (m3/s)
B

1

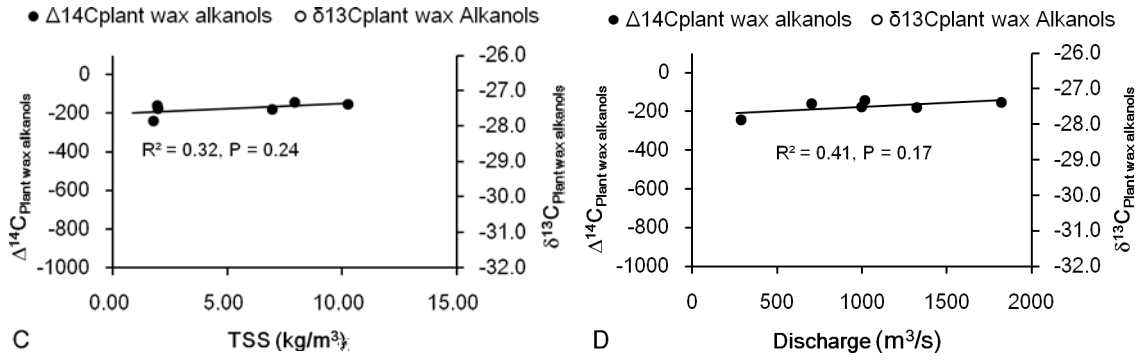
● Δ14Cplant wax alkanols ○ δ13Cplant wax Alkanols
R² = 0.32, P = 0.24
Δ14CPlant wax alkanols
δ13CPlant wax alkanols
TSS (kg/m3)
C
● Δ14Cplant wax alkanols ○ δ13Cplant wax Alkanols
R² = 0.41, P = 0.17
Δ14CPlant wax alkanols
δ13CPlant wax alkanols
Discharge (m3/s)
D

2

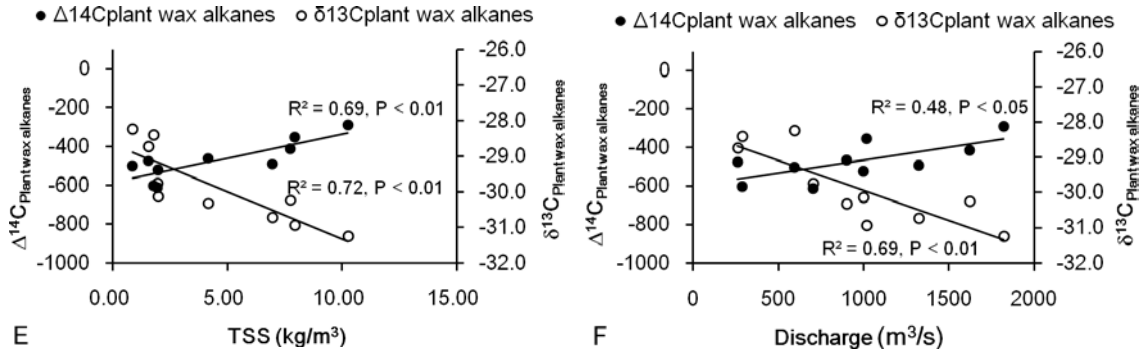
● Δ14Cplant wax alkanes ○ δ13Cplant wax alkanes
R² = 0.69, P < 0.01
R² = 0.72, P < 0.01
Δ14CPlant wax alkanes
δ13CPlant wax alkanes
TSS (kg/m3)
E
● Δ14Cplant wax alkanes ○ δ13Cplant wax alkanes
R² = 0.48, P < 0.05
R² = 0.69, P < 0.01
Δ14CPlant wax alkanes
δ13CPlant wax alkanes
Discharge (m3/s)
F

3

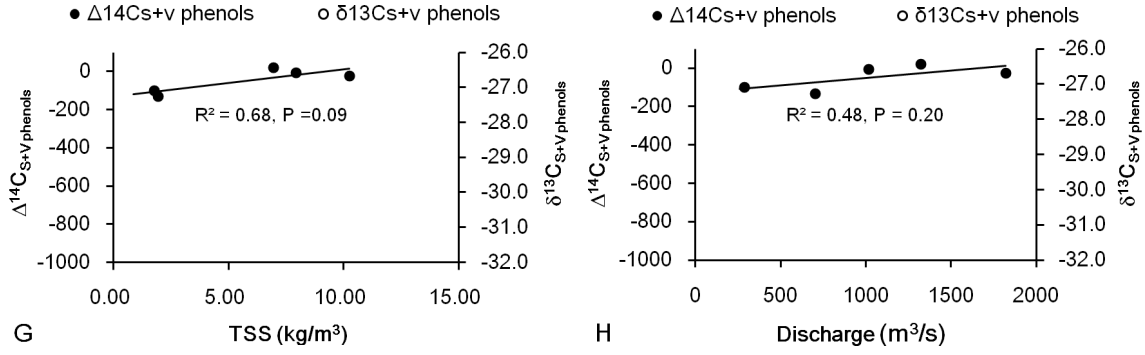
● Δ14Cs+v phenols ○ δ13Cs+v phenols
R² = 0.68, P =0.09
Δ14CS+V phenols
δ13CS+V phenols
TSS (kg/m3)
G
● Δ14Cs+v phenols ○ δ13Cs+v phenols
R² = 0.48, P = 0.20
Δ14CS+V phenols
δ13CS+V phenols
Discharge (m3/s)
H

4

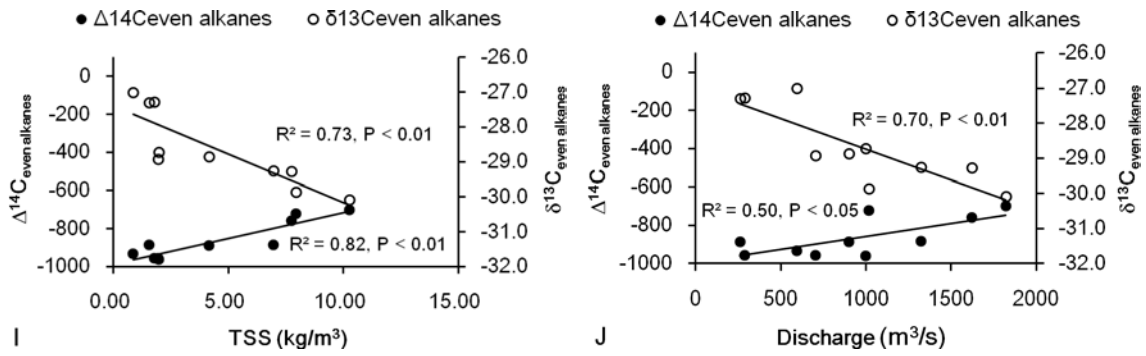

Fig. S3. Plots of typical biomarker stable carbon (open circles) and radiocarbon (filled circles) isotopic compositions *v.s.* monthly discharge and monthly TSS at the Lijin hydrodynamic station. (a) and (b) are for plant wax-derived *n*-FAs ($C_{26+28+30}$), (c) and (d) are for plant wax-derived *n*-alkanols ($C_{24+26+28}$), (e) and (f) are for plant wax-derived *n*-alkanes (C_{29+31}), (g) and (h) are for lignin-derived phenols (syringyl plus vanillyl), (i) and (j) are for long-chain even-carbon-numbered *n*-alkanes ($C_{26+28+30+32}$).

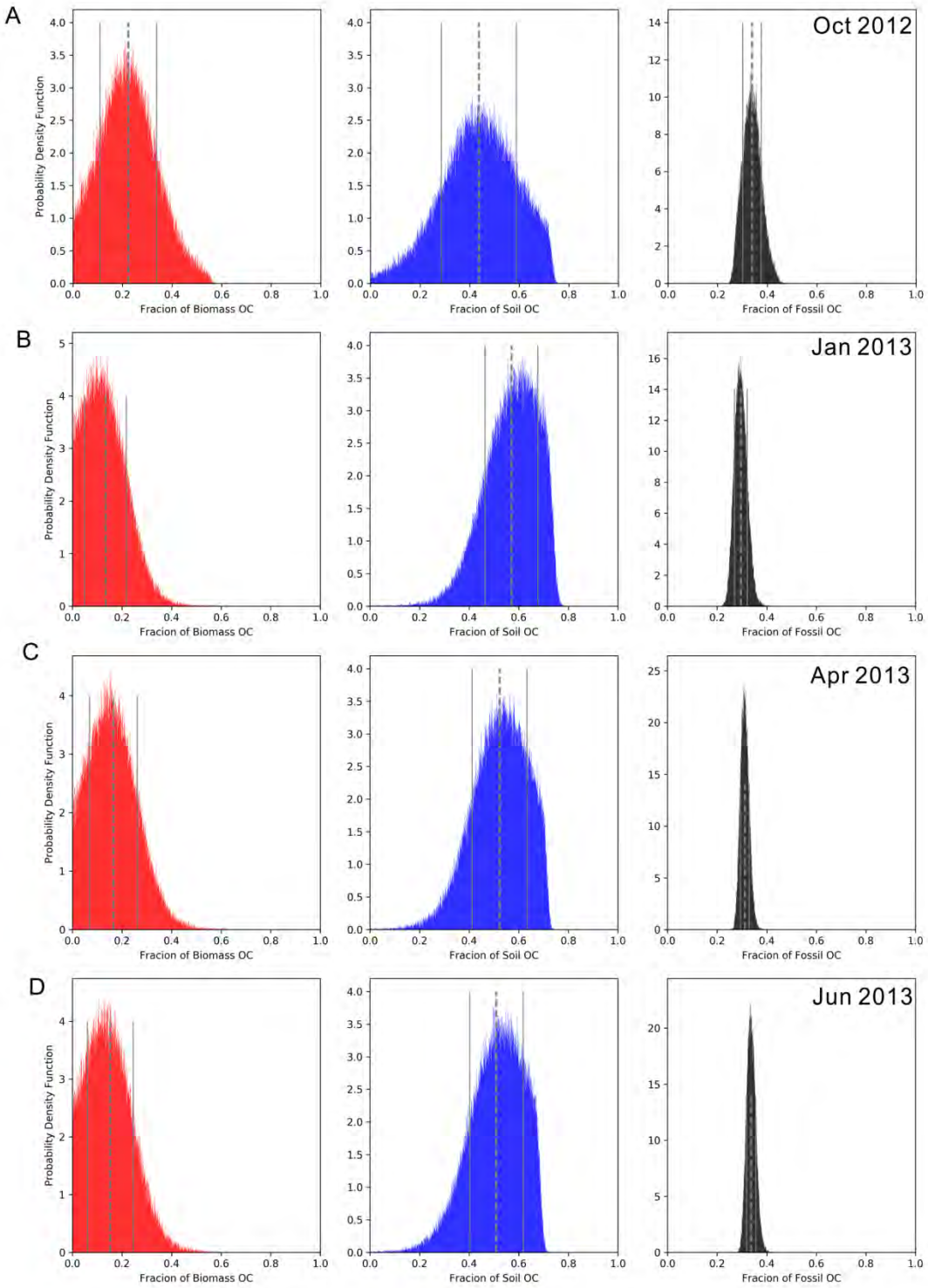

Fig. S4. Examples of Monte Carlo probability density functions for the fractions f_B, f_S and f_F to the POC from the Yellow River at different times: (a) October 2012, (b) January 2013, (c) April 2013 and (d) June 2013. Dashed vertical lines show the mean values plus and minus one standard deviation (vertical lines).

Tables

Table S1. Coupled isotope mass balance results from the Monte Carlo source apportionment calculations for the fractional contributions of modern biomass OC (f_B), pre-aged soil OC (f_S) and fossil OC (f_F) in the Yellow River SPM. The end-members and the standard deviations used in the simulations are specified in the table footnotes, and further explained and referred to in the main text.

Month	Season	Fractions		
		f_B	f_S	f_F
2011				
June*	Summer	0.17±0.10	0.48±0.13	0.35±0.03
September	Autumn	0.16±0.10	0.51±0.13	0.32±0.03
November	Autumn	0.19±0.10	0.51±0.13	0.30±0.03
2012				
January	Winter	0.17±0.10	0.53±0.13	0.30±0.03
April	Spring	0.16±0.10	0.52±0.13	0.32±0.03
June	Summer	0.22±0.13	0.49±0.15	0.29±0.02
June*	Summer	0.20±0.11	0.49±0.13	0.32±0.03
October	Autumn	0.22±0.11	0.44±0.15	0.34±0.04
2013				
January	Winter	0.13±0.08	0.57±0.11	0.30±0.03
April	Spring	0.17±0.10	0.52±0.11	0.31±0.02
June	Summer	0.18±0.10	0.52±0.12	0.30±0.02
July*	Summer	0.15±0.09	0.51±0.11	0.34±0.02

[a] End-member values used are the weighted abundance average isotopic compositions of *n*-$C_{16,18}$ FAs in specific SPM samples: corrected $\delta^{13}C$ after $\delta^{13}C_{bulk} - \delta^{13}C_{biogenic\ lipid}$ fractionation -22.61 to -20.46‰, with standard deviation of 1.00 to 1.03‰; $\Delta^{14}C$ −83 to +85‰, with standard deviation of 6 to 9‰.

[b] End-member values used are weighted-abundance-average isotopic compositions of *n*-$C_{26,28,30}$ FAs in specific SPM samples: corrected $\delta^{13}C$ after $\delta^{13}C_{bulk} - \delta^{13}C_{biogenic\ lipid}$ fractionation -25.72 to -24.72 ‰, with standard deviation of 1.00 to 1.02‰; $\Delta^{14}C$ −244 to −172‰, with standard deviation of 7 to 14‰.

[c] End-member values used are weighted-abundance-average isotopic compositions of *n*-$C_{26,28,30}$ *n*-alkanes in winter

and spring SPM samples: corrected $\delta^{13}C$ after $\delta^{13}C_{bulk}-\delta^{13}C_{petrogenic\ lipid}$ offset −22.00‰, with standard deviation of 1.07‰; $\triangle^{14}C$ −1000‰, with standard deviation of 21‰.